



Original Article

Comparison of mechanical disturbance in soft sediments due to tickler-chain SumWing trawl vs. electro-fitted PulseWing trawl

Jochen Depestele^{1,*}, Koen Degrendele², Moosa Esmaili³, Ana Ivanović³, Silke Kröger⁴, Finbarr G. O'Neill⁵, Ruth Parker⁴, Hans Polet¹, Marc Roche², Lorna R. Teal⁶, Bart Vanelslander¹, and Adriaan D. Rijnsdorp⁶

¹Fisheries Research Group, Flanders Research Institute for Agriculture, Fisheries and Food (ILVO), Ankerstraat 1, 8400 Oostende, Belgium

²Federal Public Service Economy, Energy – Continental Shelf, North Gate 4B26, Koning Albert II-laan 16, B-1000 Brussels, Belgium

³School of Engineering, Fraser Noble Building, University of Aberdeen, Aberdeen AB24 3UE, UK

⁴Lowestoft Laboratory, Centre for Environment, Fisheries and Aquaculture Science (Cefas), Pakefield Road, Lowestoft, Suffolk, NR33 0HT, UK

⁵National Institute of Aquatic Resources (DTU – AQUA), Technical University of Denmark, Willemoesvej 2, 9850 Hirtshals, Denmark

⁶Wageningen Marine Research, Wageningen UR, PO Box 68, 1970 AB IJmuiden, The Netherlands

*Corresponding author: tel: +32 59 56 98 38; e-mail: jochen.depestele@ilvo.vlaanderen.be

Depestele, J., Degrendele, K., Esmaili, M., Ivanović, A., Kröger, S., O'Neill, F. G., Parker, R., Polet, H., Roche, M., Teal, L. R., Vanelslander, B., and Rijnsdorp, A. D. Comparison of mechanical disturbance in soft sediments due to tickler-chain SumWing trawl vs. electro-fitted PulseWing trawl. – ICES Journal of Marine Science, 76: 312–329.

Received 1 March 2018; revised 12 July 2018; accepted 12 July 2018; advance access publication 20 September 2018.

Tickler-chain SumWing and electrode-fitted PulseWing trawls were compared to assess seabed impacts. Multi-beam echo sounder (MBES) bathymetry confirmed that the SumWing trawl tracks were consistently and uniformly deepened to 1.5 cm depth in contrast to 0.7 cm following PulseWing trawling. MBES backscatter strength analysis showed that SumWing trawls (3.11 dB) flattened seabed roughness significantly more than PulseWing trawls (2.37 dB). Sediment Profile Imagery (SPI) showed that SumWing trawls (mean, SD) homogenised the sediment deeper (3.4 cm, 0.9 cm) and removed more of the oxidised layer than PulseWing trawls (1 cm, 0.8 cm). The reduced PulseWing trawling impacts allowed a faster re-establishment of the oxidised layer and micro-topography. Particle size analysis suggested that SumWing trawls injected finer particles into the deeper sediment layers (~4 cm depth), while PulseWing trawling only caused coarsening of the top layers (winnowing effect). Total penetration depth (mean, SD) of the SumWing trawls (4.1 cm, 0.9 cm) and PulseWing trawls (1.8 cm, 0.8 cm) was estimated by the depth of the disturbance layer and the layer of mobilized sediment (SumWing = 0.7 cm; PulseWing trawl = 0.8 cm). PulseWing trawls reduced most of the mechanical seabed impacts compared to SumWing trawls for this substrate and area characteristics.

Keywords: beam trawl, biogeochemistry, habitat impacts, particle size distribution, penetration depth, pulse trawl, seafloor integrity, sediment resuspension

Introduction

Demersal otter trawls and beam trawls are the most widely used fishing gears to catch bottom dwelling fish, crustaceans, and bivalves (FAO, 2016; Cashion *et al.*, 2018) and are the most widespread source of physical disturbance to marine habitats (Oberle

et al., 2016; Eigaard *et al.*, 2017; Kroodsmas *et al.*, 2018). The development and implementation of ecosystem-based management strategies increasingly require assessments of bottom trawling impacts on the seabed. Risk-based assessments are an appropriate tool for this purpose. These and others are being developed for

the implementation of the European Marine Strategy Framework Directive, Descriptor 6 “Sea-floor integrity” (Rijnsdorp *et al.*, 2016; EU, 2017).

The risk of a significant adverse impact on the sea-floor (seabed) depends on (i) the likelihood of exposure and (ii) sensitivity of the seabed to fishing activities (Knights *et al.*, 2015). The likelihood of exposure relates to the overlap of distribution of habitat types and fishing effort (Eigaard *et al.*, 2017), while “sensitivity” depends on the ability to withstand fishing pressure and recover from the damage imposed (Tyler-Walters *et al.*, 2009; Depestele *et al.*, 2014). Quantifying impact is difficult but approaches are emerging that express impact as a function of mortality and the recovery rate (Pitcher *et al.*, 2017). Mortality is defined as the proportion of seabed biota killed by a single trawl pass. Mortality is very difficult to estimate due to the high spatial variability of benthic organisms (Collie *et al.*, 2000; Kaiser *et al.*, 2006; Løkkeborg, 2007; Hiddink *et al.*, 2017; Sciberras *et al.*, 2018). Measuring the trawling penetration depth is likely to be a cost-effective alternative to estimate the direct mortality imposed by bottom trawling, and allows benthic impacts across fishing gears to be compared (Eigaard *et al.*, 2016; Hiddink *et al.*, 2017; Pitcher *et al.*, 2017; Sciberras *et al.*, 2018). These novel insights set the baseline for assessing trawling impact, but require more detail at the level of different gear types to enable implementation in fisheries management (Kaiser *et al.*, 2016). Different demersal gear types are designed to have different levels of seabed contact or penetration, depending on the target species, their catching stimulus and seabed type. These factors contribute to different penetration depths, but have until now only been assessed for generic gear designs (Eigaard *et al.*, 2016; Sciberras *et al.*, 2018). Different gear configurations and the quantification of their potential benefits for mitigation of seabed impacts, cannot be ignored any longer and were identified as one of the top 10 knowledge priorities for managing seabed impact (Kaiser *et al.*, 2016).

The flatfish-directed trawler fleet in the North Sea has evolved over the last decade and used different gear configurations (Haasnoot *et al.*, 2016). Conventional tickler-chain trawls tow a number of chains over the seabed to chase flatfish out of the seabed (Rijnsdorp *et al.*, 2008). The net is opened horizontally by a steel bar (the beam) supported by two trawl shoes at each end to maintain the beam at a constant height above the seabed and maintain the vertical opening of the net. In pulse trawls, the tickler chains are replaced by electrodes that induce a cramp response that bends the fish into a U-shape, thus allowing them to be scooped up by the ground gear (Soetaert *et al.*, 2015a; de Haan *et al.*, 2016). The pulse trawls are towed at a lower speed, and may catch sole more selectively and reduce discards of benthos (van Marlen *et al.*, 2014). The beam and the two trawl shoes of the conventional tickler-chain trawl and the pulse trawl may be replaced by a wing-shaped foil with a “nose” in the centre. This wing-shaped foil was designed to reduce drag in the water and on the seabed. A tickler-chain trawl using a foil is called a “SumWing” trawl, while a trawl using the foil in combination with electric pulses is called a “PulseWing” trawl. In 2010, 30% of the Dutch flatfish-directed trawler effort was represented by beam trawls using the SumWing with tickler chains, 8% using electric pulses and 62% using the conventional beam trawl. In 2016, 12% of the effort came from SumWing trawls, 83% came from pulse trawls, while only 5% was exerted by conventional beam trawls [www.agrimate.nl (last accessed 7 May 2018)]. In 2016, 19% of the pulse trawls used a steel bar with shoes

as opposed to the wing-shaped foil (PulseWing trawl) to open the net.

In this study, we examined differences in seabed impacts between two gear configurations used to target flatfish [Dover sole (*Solea solea*) in particular]. We compared the mechanical impact on the seabed of a SumWing trawl with a PulseWing trawl, with a particular focus on the comparison of penetration depths. The penetration depth of a trawl is difficult to quantify. The passage of a trawl disturbs the top layer of the sediment, which can (i) remain in the same location, (ii) be compressed or compacted, (iii) be laterally displaced (Gillkinson *et al.*, 1998; Ivanović and O’Neill, 2015), or (iv) be mobilized and carried away from the area to a distance dependent on the particle size and bottom currents (Depestele *et al.*, 2016; Mengual *et al.*, 2016). Sediment working, mobilization and transport leads to sediment erosion (Pilskaln *et al.*, 1998; Palanques *et al.*, 2001; Durrieu de Madron *et al.*, 2005), altered seabed morphology (Eleftheriou and Robertson, 1992; Schwinghamer *et al.*, 1998; Currie and Parry, 1999), and changes in the lithological and geochemical characteristics of the seabed (Duplisea *et al.*, 2001; Puig *et al.*, 2012; Oberle *et al.*, 2018). We carried out a field experiment using complementary sampling approaches to improve our understanding of the acute changes to the seabed by two commercial trawl types in the North Sea.

Material and methods

Background to this study

In Depestele *et al.* (2016) we compared the seabed impact of bottom trawls using tickler chains vs. electric pulses to catch flatfish in the North Sea. This study elaborates on the previous findings in 2 main ways. First, Depestele *et al.* (2016) focused on one branch of the flatfish-directed trawler fleet, i.e. “euro-cutter” vessels with engine power below 300 HP (≤ 221 kW), and access to coastal waters between 3 and 12 nautical miles, including the Plaice Box (Mills *et al.*, 2007; Rijnsdorp *et al.*, 2008; Beare *et al.*, 2013). This study focused on the other branch, the large trawler fleet with engine power >300 HP, operating in offshore waters with heavier and larger trawls. The main differences in gear parameters and location characteristics of two fleets are reflected in both case studies (Supplementary Table S1; Lindeboom and de Groot, 1998).

The other differences, despite the analogous modelling approaches in both case studies, were experimental design, sampling equipment, and studied parameters differed (Supplementary Table S1). Depestele *et al.* (2016) focused on bathymetrical changes using the multi-beam echo sounder (MBES), but could not directly compare the effects of tickler-chain and pulse trawling due to differences in trawling intensities at the experimental sites. In that study, we measured sediment mobilization *in situ* using the LISST-100X, which was not deployed in this study. In this study, we used MBES bathymetry data to directly compare one passage of a SumWing trawl vs. a PulseWing trawl. We additionally analysed the MBES backscatter data and collected ground truthing data. Sediment samples were collected using a box corer and were analysed to quantify the changes in sediment sorting. The depth of disturbance and biogeochemical changes to cross-sections of the seabed were estimated using Sediment Profile Imagery (SPI) after trawling at the same intensities (Rhoads and Cande, 1971; Teal *et al.*, 2008, 2009).

Study area

The study area was located between 29 and 33 m depth in the south-western part of the Frisian Front (southern North Sea, between 53.5692–53.5859°N and 4.2664–4.2999°E). The Frisian Front is a transitional zone in the southern North Sea, located between the shallow, sandy Southern Bight and the deeper, muddy Oyster Grounds (Figure 1). The seabed in this area consists of fine sand with median grain sizes in the range of 154–163 μm and silt fractions between 12 and 17% (Bockelmann *et al.*, 2018; see “Particle size distributions and depth of sediment reworking” section). Fine sediment particles settle in this area because tidal currents drop below the critical water velocity (Creutzberg *et al.*, 1984; Stanev *et al.*, 2009). Deposition consists of particulate matter that is transported through the East Anglian turbidity plume and from locally produced phytodetritus and results in a sediment with elevated concentrations of silt, organic carbon, and phytopigments (Amaro *et al.*, 2007).

Fishing gear

The impact of a 12 m SumWing trawl and of a 12 m PulseWing trawl was studied. The SumWing trawls were deployed from the FV “Helena Elisabeth” (TX 29) and the PulseWing trawls from the FV “Biem van der Vis” (TX43). Both fishing vessels had a length overall (LOA) of ~ 40 m and a main engine power of approximately 1 500 kW. The vessels deployed a pair of 12 m wide trawls from the outrigger booms, which are kept open by a wing-shaped foil with a “nose” in the centre instead of the conventional cylindrical beam with two trawl shoes (Supplementary Figures S1 and S2). The dimensions of the wing-shaped foils did not differ.

The main differences between the gears were related to the stimuli to catch the fish (tickler chains vs. electrodes), the geometry of the net opening of the trawl, the ground gears and the nets used (Figure 2 and Supplementary Figure S2). Both trawls had a cod-end with 80 mm stretched diamond-shaped mesh opening as used in the commercial sole fishery (Bayse *et al.*, 2016; Uhlmann *et al.*, 2016), but the SumWing trawl net used during the experiment was lighter than most trawl nets used in the fleet (M. Drijver, skipper of TX29, pers. comm.). The catching process of the SumWing trawl was based on mechanical disturbance by the tickler chains, which are rigged in the V-shaped net opening, perpendicular to the towing direction. The SumWing trawls were towed at speeds of ~ 6 kn with a scope ratio of 3 (ratio of warp length to water depth). The total gear weighted nearly 3.1 t in air or 1.6 t in water (HfK Engineering, 2018). Eight tickler chains with a chain link diameter of between 18 and 24 mm and a total length between 18.6 and 26 m were attached to the wing. In addition, 9 tickler chains were attached to the middle part of the ground gear. Their length varied between 6 and 14 m, with a chain link diameter was between 13 and 16 mm. Three shorter tickler chains (4.5–5 m) with a diameter of 16 mm were attached to the aft part of the ground gear (Figure 2). The ground gear consisted of a 37 m long chain with rubber discs with a diameter between 18 and 28 cm covering the chain over a 7.8 m centre section. The electrodes of the PulseWing trawl were rigged in a longitudinal direction into the square-shaped mouth opening of the trawl net. The PulseWing trawls were towed at fishing speeds of ~ 5 kn with a scope ratio of 3 (Figure 2). The total gear weighted 2.8 t in air or 1.4 t in water. A total of 27 electrode modules were attached to the wing-shaped foil and the ground gear. The commercial electrodes (HfK Engineering) have a diameter of 3.3 cm

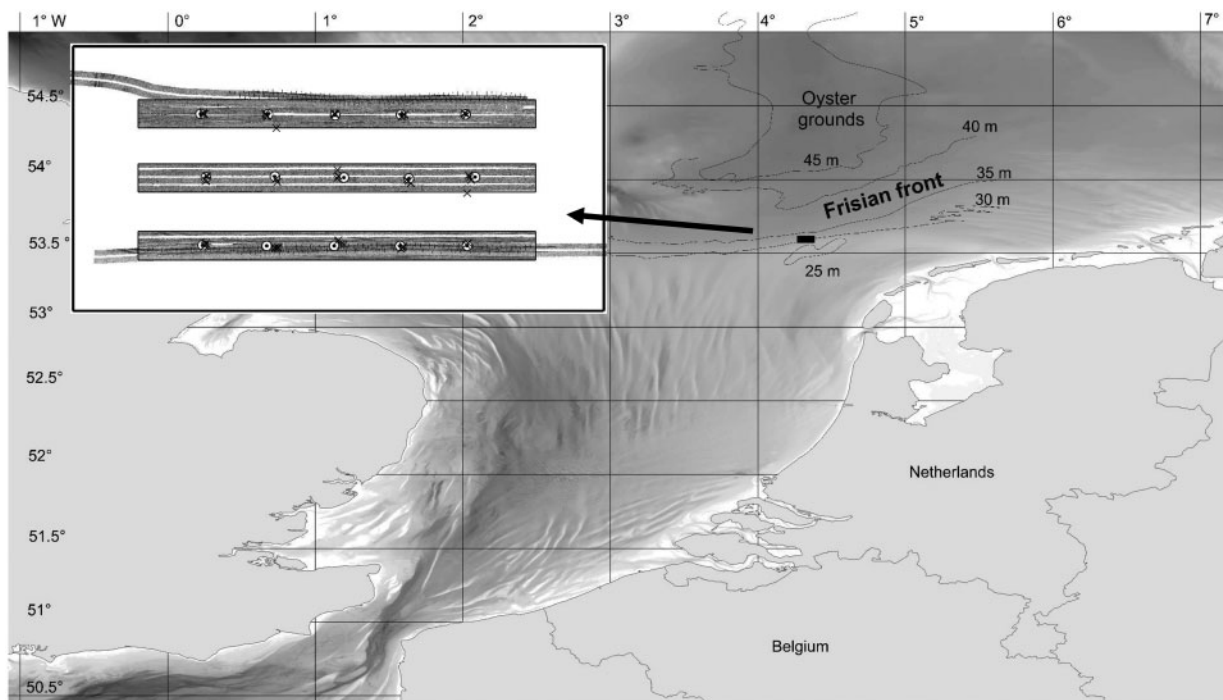


Figure 1. The study area was located in the southwestern part of the Frisian Front. Experimental sites were designated for PulseWing trawling (north), SumWing trawling (south), and control (no trawling). Each experimental site was sampled before and after trawling using a multi-beam echo sounder (total area), a box corer (circles; $N = 5$), and a sediment profile imager (crosses; $N = 20$).

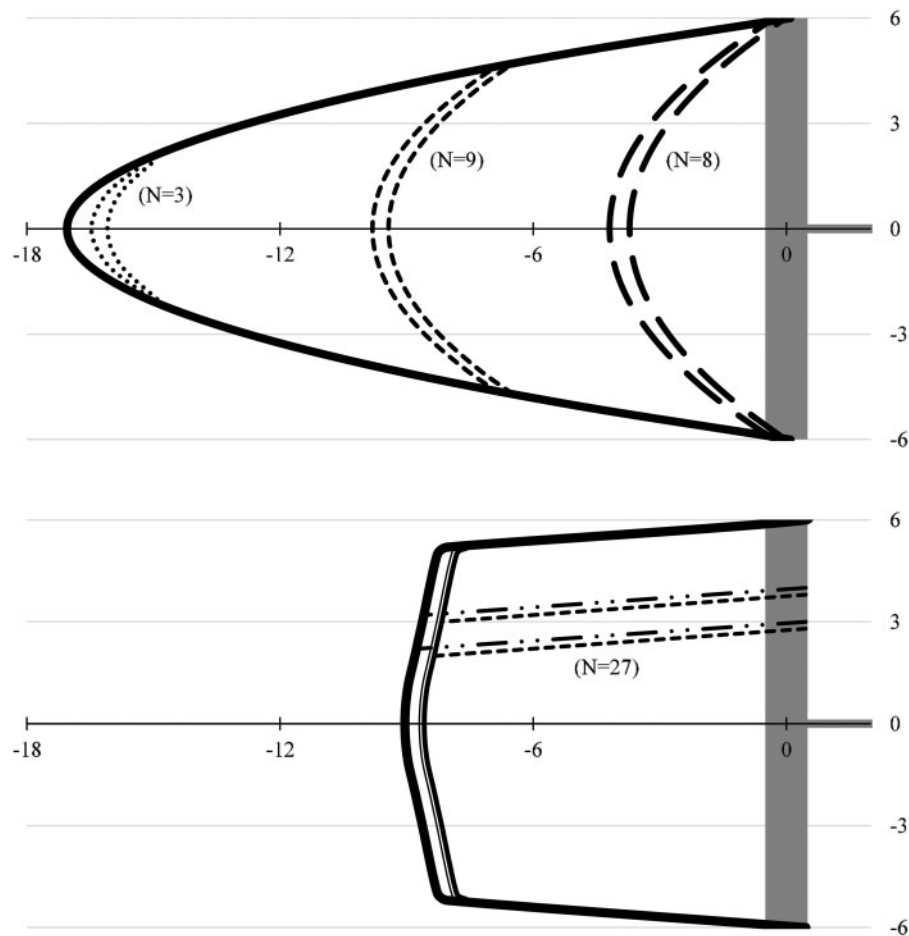


Figure 2. Gear components of the SumWing trawl (upper panel) and PulseWing trawl (lower panel). Tickler chains with a chain link diameter between 18 and 24 mm are attached to the SumWing, whereas the tickler chains (13–16 mm) are attached to the ground gear. The electrode modules consist of tension relief cords (dashed line, $d = 8\text{--}10\text{ cm}$) and an electrode (dashed-dotted line, $d = 3.3\text{ cm}$) (Supplementary Figures S1 and S2). Tension relief cords are attached to the first ground rope, while electrodes are attached to the second ground rope to prevent damage. N indicates the number of tickler chains or electrode modules.

and produce a 60 Hz pulsed bipolar current at 45–50 V with a 0.36 μs pulse duration (Soetaert *et al.*, 2015a; de Haan *et al.*, 2016). A disc-protected rope (of diameter 8–10 cm) is rigged alongside each electrode to withstand the tension from towing the gear over the seabed (hereafter called “tension relief cords”). The mouth of the PulseWing trawl had a square-shaped opening, resulting from two disc-protected chains that were running parallel to the towing direction at the sides of the mouth opening and from two ground ropes, that are both running perpendicular to the towing direction and rigged just in front of the trawl net mouth opening (Figure 2 and Supplementary Figure S2). The tension relief cords were attached to the first rubber disc ground gear (diameter = 12 cm), while the net was attached to the second rubber disc ground gear (diameter = 20 cm) (Supplementary Figure S2).

Experimental fishing and experimental sites

Acute fishing disturbance by each trawl type was evaluated in a controlled experimental design. We chose 3 sites of $200 \times 2\,800\text{ m}$ (0.56 km^2) each, located 250 m apart (Figure 1). The PulseWing trawl was fishing in the northern site and the

SumWing trawl in the southern site. No fishing took place in the central site, which was used as a control. Samples were taken from this site to measure the influence of factors other than fishing such as waves and currents (Figure 3). The experimental sites were located on a gentle slope with median grain sizes of 154, 162, and 169 μm in the PulseWing, control and SumWing trawl sites, respectively. Most particle sizes (down to 10 cm depth) classified as fine sand (125–250 μm): 59% in the PulseWing site, 63% in the control and 70% in the SumWing site, with a respective silt fraction of 17, 13, and 12%. The fine sand fraction in the top layers was similar to the deeper layers, with a slight decrease (5%) in the SumWing site. The mean silt fraction was lower in the top layers than in the deeper layers but its relationship with depth differed between sites.

Six hauls of varying haul duration took place on 10 June 2014 (PulseWing trawl between 8:50 and 15:00; SumWing trawl between 9:26 and 14:24). Fishing operations were carried out as similarly as possible, resulting in 13 passages along the length of each site that represented an equal swept area of 0.872 km^2 and a fishing intensity of 156% ($= 0.872/0.56\text{ km}^2$) for each gear in their respective experimental site. Observations from the

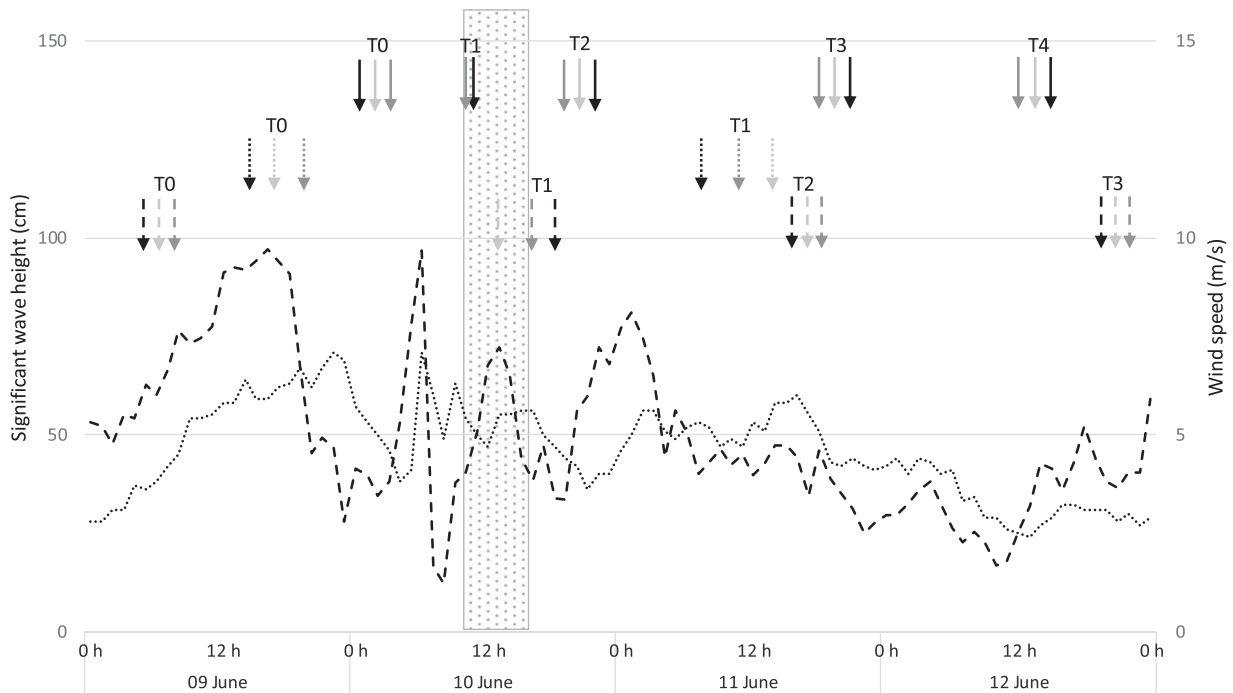


Figure 3. Multibeam echo sounder (full line arrows), Sediment Profile Imagery (dashed arrows), and box corer (dotted arrows) measurements took place before fishing (grey rectangle) and at various times T after fishing with the SumWing trawl (dark grey arrows) or the PulseWing trawl (black arrows). Light grey arrows indicate sampling in the control site where no fishing took place. Mean (\pm SD) wind speed (dashed line) and significant wave height (dotted line) indicate a gentle breeze (4.9 ± 2.0 m/s; 16.0 ± 12.0 m) with excellent sampling conditions, particularly after fishing.

Research Vessel (RV) during the entire experimental period (9–12 June 2014) ensured that no fishing had taken place in the experimental sites other than experimental trawling. Previous trawling disturbances in the experimental sites were limited, as evaluated from prior inspection using the multi-beam echo sounder. Historic disturbance by bottom-contacting gears in the area was also low, varying between once every 10 years to once every 2 years (Supplementary Figure S3; Eigaard *et al.*, 2016, 2017).

Data collection methods

The effects on the seabed were measured using three observation techniques: (i) the multi-beam echo sounder (MBES) for assessing changes in the sedimentary interface using both bathymetrical and backscatter strength data, (ii) Sediment Profile Imagery (SPI) for identifying geochemical changes, and (iii) box corer sampling for particle size analysis. These measurements were collected in all experimental sites before and after fishing during mild weather conditions (significant wave heights <75 cm; wind speeds <10 m/s) (see Figure 3).

Multi-beam echo sounder

Acoustic measurements were performed with the Kongsberg EM2040 single head multi-beam echo sounder (MBES) mounted on the RV Simon Stevin (Depestele *et al.*, 2016). The experimental sites were surveyed before any experimental fishing disturbance began (T_0). MBES recordings were obtained by following the fishing vessel at a close distance (<300 m) during its first trawling passage to estimate changes in seabed bathymetry immediately after fishing (T_1 ; <0.5 h after fishing). Additional MBES surveys were conducted within 12 h (T_2), after 1 day (T_3), and

after 2 days (T_4) (Table 1). All monitoring occurred with a MBES frequency of 320 kHz. Survey lines started and ended 30–50 m outside the experimental sites and were conducted at a speed of 8 kn and orientated parallel to the longest side of the sites with an approximate overlap of 30%. MBES measurements across all entire experimental sites were used to assess changes in backscatter strength (BS). BS is used as a proxy to characterize the seabed: higher BS values represent coarse, rough interface with many scatterers (e.g. hard-bodied organisms) while lower BS values represent softer sediment with reduced roughness and fewer scatterers (Ferrini and Flood, 2006).

Seabed bathymetry

A high resolution (0.5 by 0.5 m) digital elevation model of the seabed was created for the MBES survey lines at T_0 and T_1 by filling an empty grid with validated soundings from the nearest ping in SonarScope (Ifremer, 2016). Trawl tracks were visually detected in the GIS (ArcGIS) on the 0.5×0.5 m BS mosaic (section below). The bathymetrical changes due to fishing were assessed from water depth measurements inside and outside the trawl track. Measurements were selected from equally spaced (20 m) cross-sections ($N = 82$ for PulseWing trawl; $N = 120$ for SumWing trawl) with a mean of >25 measurements inside the track and >40 outside the track. The bathymetric profile of each cross-section was corrected for its slope using ordinary least squares regression. The slope-corrected depth measurements inside and outside the track were then compared to a non-parametric Friedman rank sum test following a single factor (water depth) within subject (cross-section) design (Depestele *et al.*, 2016). Statistical differences between water depths inside

Table 1. Backscatter values and statistical differences between time intervals (T0, T2, T3, T4) and experimental sites (pulse: PulseWing trawling; control: no fishing; tickler: SumWing trawling).

Site	Time interval	Description of time intervals	Time lapse (h)	Backscatter values (dB)				Statistical differences at	
				Mean	SD	Lower CI	Upper CI	$p < 0.05$	$p < 1 e^{-6}$
Tickler	T0	Before fishing	–9h48	–36.99	2.34	–37.10	–36.89	fg	d
Pulse	T0	Before fishing	–7h32	–36.94	2.28	–37.05	–36.84	g	d
Control	T0	Before fishing	–8h57	–36.92	2.22	–37.02	–36.82	g	d
Tickler	T2	<12 h	5h02	–40.10	2.25	–40.20	–39.99	a	a
Pulse	T2	<12 h	5h02	–39.31	1.87	–39.39	–39.22	b	b
Control	T2	<12 h	5h02	–37.32	1.68	–37.40	–37.24	e	d
Tickler	T3	1 d	30h20	–39.16	2.45	–39.28	–39.05	b	b
Control	T3	1 d	30h20	–37.23	2.33	–37.34	–37.13	ef	d
Pulse	T3	1 d	30h20	–38.40	2.21	–38.50	–38.31	c	c
Tickler	T4	2 d	46h36	–39.07	2.54	–39.19	–38.96	b	b
Pulse	T4	2 d	46h36	–38.12	2.34	–38.23	–38.01	d	c
Control	T4	2 d	46h36	–37.26	2.36	–37.36	–37.15	e	d

Sites and time intervals with a different letters are statistically different at p -values of 0.05 or $1e^{-6}$. Rows are ordered from low to high backscatter values to show which gear and time interval caused the most change in BS. SD, standard deviation; CI, 95% confidence interval.

and outside the trawl tracks were tested for the SumWing and PulseWing trawls at T0 and T1. The deepening of the trawl track was then assessed by subtracting the cumulative depth distribution after fishing from the cumulative depth distribution before fishing. In other words, we first tested whether trawling was conducted on a “flat” surface, i.e. the locations to be trawled were not positioned shallower or deeper than their surroundings. We then assumed that any differences in water depths found in the trawl track locations at T1 were due to the passage of the trawl.

Seabed backscatter strength

A BS mosaic of 0.5 by 0.5 m resolution was computed for each MBES line. An angular compensation was applied using the mean BS level—incident angle curves computed independently for each line. Only BS values derived from oblique incident angle, inside the angular interval of 30–50°, have been considered. The resulting BS mosaics (by line compensated) were merged by experimental site (PulseWing trawl, control, and SumWing trawl) and time interval (T0, T2, T3, and T4). BS values from these mosaics were randomly sampled without replacement to increase computational efficiency in further analysis and eliminated as outliers (1.3% of the data) when outside 1.5 times the interquartile (25–75%) range (1.3% of the data) (Hoaglin and Iglewicz, 1987). This procedure yielded a dataset of >1 700 backscatter values per site and time interval. A linear model was applied to the backscatter values with site, time interval and their interaction as fixed effects. Visual inspection of the histogram and QQ-plot indicated normality of the residuals and a plot of the residuals vs. fitted values confirmed homogeneity of the variances, which allowed ANOVA type III analysis of the model. Significant factors ($p < 0.05$) were tested in *post-hoc* pairwise comparisons to least-square means and p -values were corrected by Tukey–Kramer adjustment for multiple comparisons.

Sediment profile imagery

An SPI camera (sediment profile imagery, Ocean Imaging Systems, North Falmouth, MA, USA) was deployed at each experimental site at four points in time: T0, T1, T2, and T3 (Figure 3).

Two replicate images of the sediment were collected at 10 locations per site (Figure 1) (for general principles, see Rhoads and Cande, 1971; Germano *et al.*, 2011). The imaging module was based around a Nikon D100 camera (2 000 × 3 000 pixels = 6 mega pixels, effective resolution = 75 × 75 µm per pixel), set to an exposure of 1/60 and a film speed equivalent to ISO 400. These *in situ* images (15 cm × 21.5 cm = 322.50 cm²) show the apparent redox potential discontinuity (arPD), which is a reliable proxy for the biological mixing depth (BMD) (Teal *et al.*, 2009; Statham *et al.*, 2018). The depth of this brownish, oxidized layer indicates when biogeochemical redox conditions allow the maximum extent of the presence of particulate iron oxide. The depth of this oxidized layer was quantified using a custom-made, semi-automated macro (modified from Solan *et al.*, 2004) within ImageJ (vs. 1.38), a Java-based public domain program developed at the US National Institutes of Health [http://rsb.info.nih.gov/ij/index.html (last accessed 8 February 2018)]. The depth of the disturbance layer was eliminated when quantifying the oxidized layer post trawling. The effects of trawling and short-time recovery time on the depth of the oxidized layer was assessed using a one-way analysis of variance (ANOVA) with time steps as sources of variation for SumWing and PulseWing trawling separately. Significance of the differences between time steps were tested using a *post-hoc* Tukey’s comparison test.

The trawling effect at T1 was further assessed using 2 additional parameters. First, surface boundary roughness (i.e. maximum minus minimum depth of penetration) was compared between sites using a one-way ANOVA (Solan and Kennedy, 2002) using a *post-hoc* Tukey’s comparison test to evaluate differences between sites. Second, the depth of the disturbance layer was analysed using a combination of visual assessment and confirmation within an expert user group. Disturbance layer depths were measured directly on hard-copy after image annotation. The potential influence of the measurements by individual experts ($n = 3$) and the effect of trawl type (SumWing vs. PulseWing trawl) on the depth of disturbance were analysed in a linear model with site, time interval, and their interaction as fixed effects. Homogeneity of the variances was visually inspected as were the residuals (histogram and QQ plot). A two-way ANOVA

type III analysis of the model was conducted using *post-hoc* Tukey's comparisons to assess differences between significant factors. The results were analysed using R 3.3.2 for Windows (R Foundation for Statistical Computing, Vienna, Austria).

Box corer sampling and particle size distributions

Sediment samples were taken in each experimental site at T0 and T1 (Figures 1 and 3) using a cylindrical box corer with a diameter of 50 cm and a height of 55 cm, equipped with a valve to prevent flushing or loss of the top layer (de Jong *et al.*, 2015). After recovery of the box corer samples the overlying water was siphoned off, and the sediment surface was carefully studied. In case of disturbance the sample was discarded and a new sample was taken. Small sub cores of 5 cm diameter were taken out of the box corers and sliced in layers of 5 mm (from 0 to 1 cm) and 10 mm (from 1 to 10 cm). Sediment samples were stored in the dark and frozen at -20°C until particle size analysis. Particle size distribution was measured using a Malvern Mastersizer 2000[®] laser diffractometer using a Hydro 2000 G wet sampling system (Malvern, UK). Main parameters applied within the Standard Operating Procedure were a material refractive index of 1.55, a dispersant refractive index of 1.33, stirrer speed at 1 000 rpm, pump speed at 2 500 rpm, 60 s of ultrasonic vibrations during 60 s of premeasurement, 15 s background time, and 15 s measurement time.

Particle size histograms were plotted before (T0) and after fishing (T1) for each experimental site using a LOESS smoother (span = 0.3) in ggplot2 for R (Wickham, 2009). The histograms were drawn for 2 depth categories: 0–1 cm and 1–4 cm. The depth categories were based on differences in mean depth of disturbance of experimental SumWing and PulseWing trawling using SPI results (see "Oxidized layer and depth of disturbance" section).

The shape of the particle size distributions was largely determined by the silt fraction ($<63\ \mu\text{m}$; 9–15%) and the fine sand fraction (125–250 μm ; 50–80%). Both of these fractions were examined in detail as a function of depth, time in relation to fishing (T0 and T1) and experimental site. The mean and standard deviation of the silt or fine sand fraction were modelled using Generalized Additive Models (GAM) with a Gaussian error distribution (Wood, 2011). Homoscedasticity and normality assumptions were evaluated through visual examination of plotted standardized residuals vs. fitted values and QQ-plots of the residuals. Models with a lower AIC were selected if the ΔAIC was >2 . The relationship with depth was first evaluated between experimental sites before fishing (T0) and between experimental sites without fishing disturbance (T0 of each site and T1 of the control site). The different relationships of the silt fraction with depth for each experimental site and time step were then compared to the experimental sites after trawling (T1).

Numerical modelling of penetration depth

Three-dimensional numerical modelling based on the finite element method ABAQUS with Explicit solution was used to simulate interaction processes between the trawls and the seabed (Esmaili and Ivanović, 2014, 2015). The trawl–seabed interactions were implemented using the Coupled Eulerian Lagrangian (CEL) method with Eulerian mesh based on the volume of fluid method (Dassault, 2014). The flow of the material through the mesh was tracked by computing its Eulerian volume fraction (EVF). The value of EVF represents the portion of material filled;

EVF = 1 indicates that the element is completely filled with the material and EVF = 0 indicates the element is devoid of the material. The seabed was modelled as elastoplastic, obeying the cap Mohr–Coulomb model criterion, having the following parameters: specific weight of $19.5\ \text{kN m}^{-3}$, Young's modulus of 10 MPa, Poisson's ratio of 0.3, cohesion intercept of 0.01 kPa, angle of internal friction, $\varphi = 32^{\circ}$ and a dilatation angle of 1° . The tri-axial test, the shear box test and the one-dimensional compaction test were performed in the laboratory to obtain these parameters. A penalty friction formulation based on Coulomb friction law was used as contact property representing the frictional behaviour between contacting bodies (Esmaili and Ivanović, 2015). The interaction of the trawls and the seabed was modelled from a reference configuration represented by a cuboid, consisting of two regions: the initial seabed material and a void region. Both regions were discretized using eight-node linear multi-material Eulerian bricks with reduced integration and hourglass control. The trawls were modelled as elastic bodies specified by elastic constants leading to large elastic stiffness. The Lagrangian (trawl) elements were discretized using four-node quadrilaterals. Their mass and rotary inertia was specified at the centre, and they were given a linear velocity in the x -direction, ramping smoothly from zero velocity to a constant value in the next step. In a simulation, the void region was initially empty but filled up with the Lagrangian (trawl) elements and material flowing into the mesh within the Eulerian domain once the passage of a trawl element is simulated. The simulations ran sufficiently long to reach quasi-static condition and were conducted for the nose of the wing-shaped foil of the SumWing and the PulseWing trawl, one single electrode and one single tickler chain with chain link diameter of 24 mm.

Modelling of sediment mobilization

The approach of O'Neill and Ivanović (2016) was applied to estimate the quantity of sediment mobilized in the wake of a gear component. Their model estimates the amount of sediment mobilized immediately behind a towed gear component in terms of the hydrodynamic drag of the gear component and the silt fraction of the sediment. It does not predict the fate of the sediment and whether it falls in the track of the component (as is likely for the larger particles) or whether it goes into suspension and is diffused or transported away by ambient currents (as is likely the case for the smaller particle sizes). In Depestele *et al.* (2016) we applied our model to a 4 m beam trawl and found a good agreement between the model predictions and field measurements.

Here, we have applied a similar methodology to measure the amount of sediment mobilized by each of the trawls of our experiments. We calculated the drag of the noses of the wing-shaped foil, the electrodes and the ground gear from experiments on similar shaped objects (Hoerner, 1965; O'Neill and Summerbell, 2016), the drag of the chains from the numerical estimates of Xu and Huang (2014), and the drag of the netting panels in the lower half of the trawl from the empirical model of MacLennan (1981). The silt fraction at each experimental site was estimated from the upper 2 cm sediment layer of the box corer samples taken at T0.

Results

Seabed bathymetry

There was no difference at T0 between the water depths inside and outside the trawl tracks at either site [SumWing trawling location: $\chi^2(df = 1)=3.6, p = 0.06$; PulseWing trawling location: $\chi^2(df = 1)=0.08, p = 0.78$]. After trawling (T1), the mean (SD) track depths were significantly deeper and were 15.1 (0.9) and 9.1 (1.6) mm for the SumWing and PulseWing trawls, respectively [SumWing trawling location: $\chi^2(df = 1)=93.63, p < 0.0001$; PulseWing trawling location: $\chi^2(df = 1)=17.61, p < 0.0001$]. The track depth was deeper for the SumWing trawl with a range of depths between 7.6 and 37.5 mm; however, the range was wider for the PulseWing trawl (8.9–59.5 mm) (Table 2; Figure 4).

Seabed backscatter strength

Seabed BS was statistically different across the experimental sites and time intervals ($F_{6, 22, 0.31}=126.7, p < 0.00001$) (Supplementary Table S2). *Post-hoc* pairwise comparisons indicated that there were no statistical differences between the BS of each experimental site before fishing, but at T2 (after fishing) BS decreased significantly by 9% following SumWing trawling and by 6% following PulseWing trawling (Table 1; Figure 5; Supplementary Table S3). In the adjacent control site, BS was reduced by 1% ($p < 0.05$) from before-fishing conditions (Table 1; Figure 5). After trawling, BS values of the experimentally fished sites increased rapidly in the direction of before-fishing conditions, but this trend attenuated after 1 day (Table 1; Figure 5).

The reduction of the BS of the control site persisted over the 2-day observation period.

Oxidized layer and depth of disturbance

SPI images from T0 conditions show the occurrence of infaunal bioturbators like *Echinocardium* spp. and *Callianassa* spp. and an oxidized/suboxic upper layer of brown particles at both SumWing and PulseWing sites. These observations are consistent with an undisturbed sediment where iron reduction (after use of oxygen, nitrate, and manganese) leads to grey colour change of the deeper sediment layers as the brown ferric coatings are lost from particles (Figure 6). The oxidized layer at T1 was intensively disturbed by both the SumWing and the PulseWing trawl. Both trawl types disturbed the upper (oxidized) layers of the sediment and created a homogenized disturbance layer in the upper parts of the sediment profile (Figures 6 and 7). The disturbance layer consisted of both brown particles from the oxidized layer and grey/black particles from below and reduced surface boundary roughness significantly following SumWing trawling in comparison to the control site ($F_{2, 58}=7.74, p < 0.01$) (Figure 7; Supplementary Tables S4 and S5). The disturbance layer was sometimes interspersed with mud clasts, particularly in the SumWing images. Reduction of the homogenized layer was greater for the PulseWing trawl (1.0 ± 0.8 cm) and often did not cover the entire SPI image width. The oxidized layer in the SumWing images was either completely removed or a marked boundary was created between the trawling-induced

Table 2. Track depth (mm) before and after SumWing (tickler) and PulseWing (pulse) trawling.

Site	Time interval	Mean (SD)	Min	Q1	Med	Q3	Max	$\chi^2(df = 1)$	p-Value
Tickler	T0	-1.6 (1.0)	32.7	5.2	-1.5	-8.5	-29.7	3.6	0.05791
Tickler	T1	-15.1 (0.9)	-9.3	-8.6	-15.2	-20.9	-37.5	93.63	$p < 0.0001$
Pulse	T0	0.2 (0.9)	31.9	5.3	-0.2	-5.3	-28.2	0.08	0.77584
Pulse	T1	-9.1 (1.6)	28.1	0.5	-7.7	-17.9	-59.5	17.61	$p < 0.0001$

Negative values indicate the deepening of the trawl track. χ^2 -values compare water depths inside and outside the trawled track.

T0, before fishing; T1, immediately following fishing; SD, standard deviation; min, minimum; Q1, first quartile; med, median; Q3, third quartile; max, maximum.

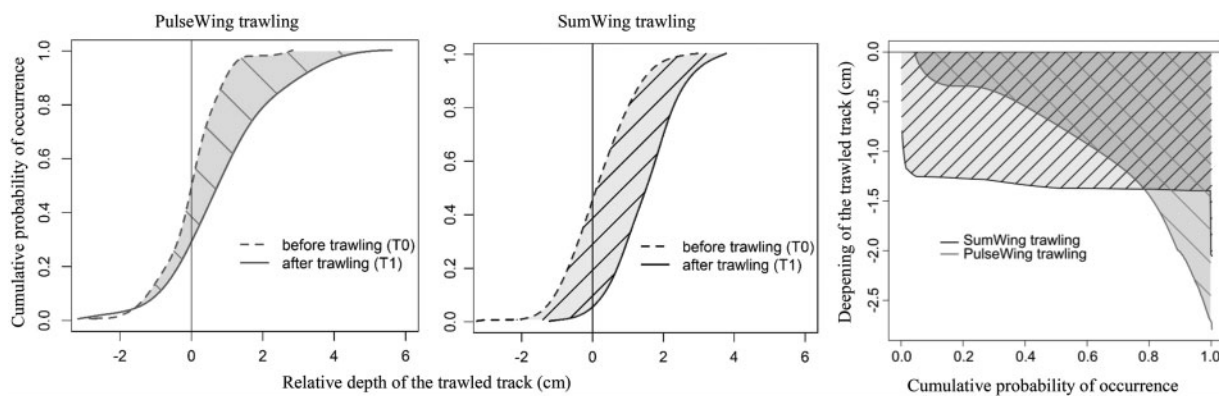


Figure 4. Relative depth of the trawled track (cm) before and after trawling (left and middle panels) and its deepening (right panel). The relative depth of the trawled track was calculated from the differences in water depths inside and outside the trawled track. These relative depths were calculated after trawling (T1, solid lines) and also before trawling (T0, dashed lines) using the locations of the trawled track from T1. Negative relative depths indicate that the trawled track was higher than its surroundings. The deepening of the trawled tracks was based on the comparison of the relative depths in the trawled track before (T0, dashed) and after (T1, solid) SumWing trawling (black lines) and PulseWing trawling (grey lines). Deepening is illustrated by the shaded areas. Please note that deepening differs from penetration depth.

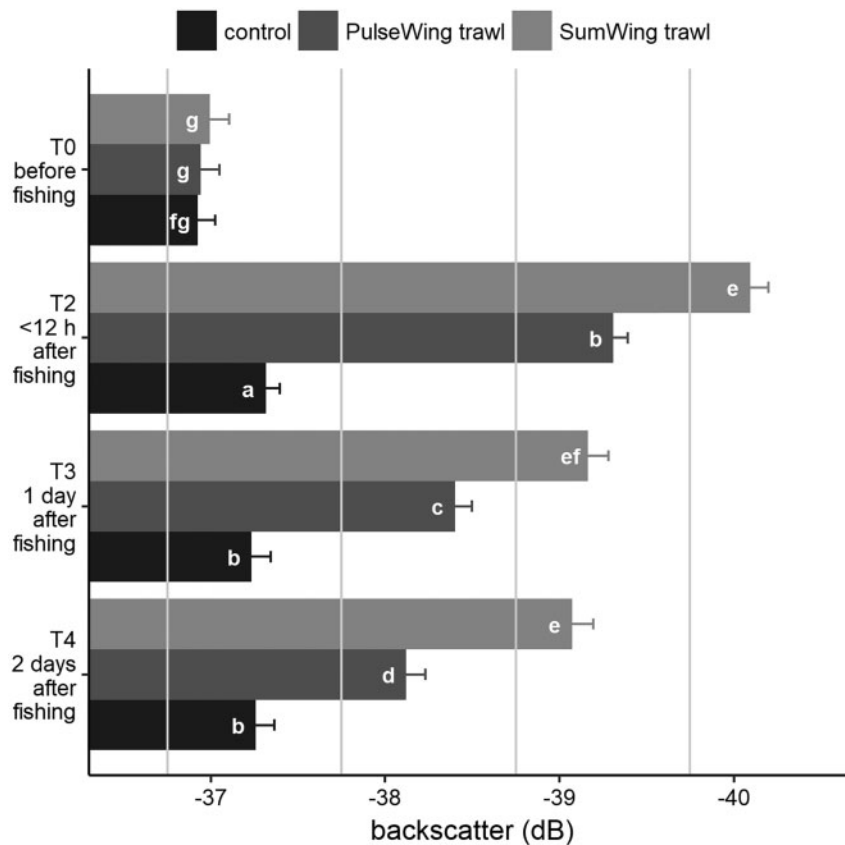


Figure 5. Absorption of sound (acoustic measurement, i.e. backscatter values in dB) of three experimental sites (PulseWing trawl, SumWing trawl, and control: no fishing) at various time intervals before and after trawling (Table 1; Figure 3). Letters denote statistical differences ($p < 0.05$) between sites and time intervals.

disturbance layer and the relic oxidized layer. The homogenized disturbance layer was more frequent and consistent across the SumWing images and was significantly deeper (3.4 ± 0.9 cm; $F_{1, 114} = 230.555$, $p < 0.001$) (Figure 8; Supplementary Tables S6 and S7). The assessment of the disturbance layer did not differ significantly between individual experts ($F_{2, 114} = 2.36$, $p = 0.259$) (Supplementary Table S6).

Depending on the trawl penetration, a remnant of the brown oxidized layer sometimes remained visible below this homogenized layer. Over time (1–2 days) the brown colour of these particles faded to grey. Also over time the homogenized layer consolidated and the oxic part of the sediment was set up again (within hours of the T2 and T3 images) and the redox clines and biological mixing were likely to be re-established. This is shown in the appearance of the iron oxidized surface layers and smoothing of the homogenized layer boundaries in T2 and T3. The oxidized layer in T0 was significantly different following SumWing trawling in T1, T2, and T3 ($F_{3, 251} = 33.7$, $p < 0.0001$) (Figure 7; Supplementary Tables S8 and S9). The time required for full recovery following tickler chain trawling exceeded the 48 h observational period. In contrast, the oxidized layer following PulseWing trawling in T1, T2, and T3, although variable, was not significantly different from T0 ($F_{3, 256} = 2.208$, $p = 0.088$) (Figure 7; Supplementary Tables S10 and S11).

Particle size distributions and depth of sediment reworking

The shift in particle size distributions between T0 and T1 in the top layer (0–1 cm) suggested a decrease in smaller particle sizes (silt fraction) and an increase in larger particle sizes (fine sand fraction) in the SumWing and PulseWing sites (Figure 9, upper rows). The T0 and T1 particle size distributions in the control site overlapped and remained largely unchanged in the top 1 cm layer. The particle size distribution in the layer between 1 and 4 cm suggested the same shift in particle size distribution in the control site as in the PulseWing site. The particle size distribution in the SumWing site, in contrast, suggested an opposite trend, which was particularly reflected by the decrease in fine sand fraction after trawling (T0 vs. T1 in Figure 9, lower rows).

The modelling exercises of 2 primary sediment fractions showed similar patterns of depth of sediment reworking. SumWing and PulseWing trawling decreased the silt fraction in the top layers, but in contrast to PulseWing trawling, the SumWing trawl also caused an increase in the mean silt fraction in the deeper layers (T1 in Figure 10, upper rows). Similar trends were reflected in the fine sand fraction. Both PulseWing and SumWing trawling increased the fine sand fraction in the top layer, but only SumWing trawling caused a decrease in fine sand in the deeper layers (Supplementary Figure S4).

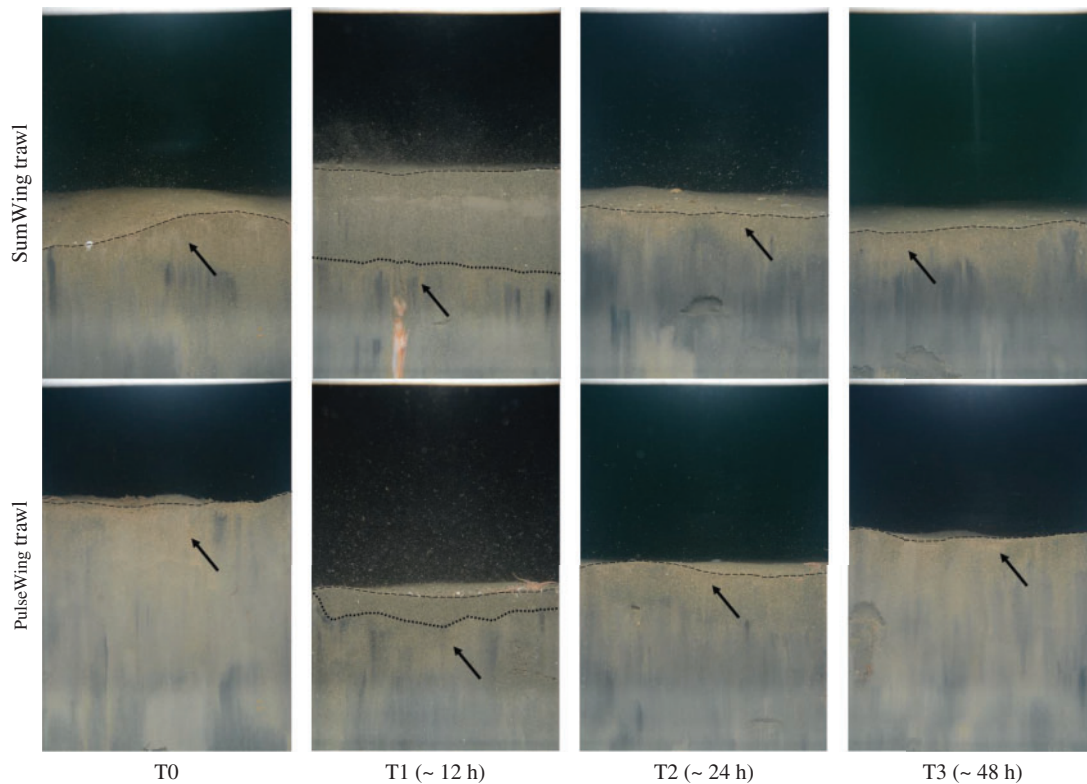


Figure 6. Selected SPI images before (T0) and after SumWing and PulseWing trawling (T1, T2, T3) (see Figure 3 for time steps). The oxidized layer (arrows) was measured downward from the surface boundaries (dashed lines). The disturbance layer is the area between the surface boundary and the marked boundary between the homogenized sediment area and the oxidized layer (dotted line in T1 images).

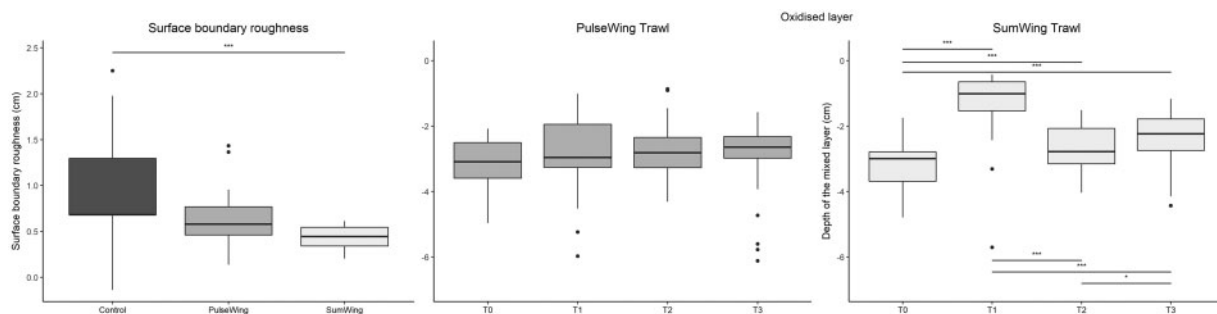


Figure 7. Surface boundary roughness at T1 conditions in the control (dark grey), PulseWing (middle grey), and SumWing (light grey) experimental sites (left panel) and depth of the oxidized layer following PulseWing trawling (middle panel) and SumWing trawling (right panel) at T0, T1, T2, and T3 conditions. Significance levels: * $p < 0.05$; ** $p < 0.01$; *** $p < 0.001$.

The depth to which both trawling methods affected the seabed was also reflected in the variability of the particle sizes before and after trawling. The variability of the silt and fine sand fraction was low in the control site before and after trawling (Figure 10 and Supplementary Figure S4). The variability in silt and fine sand fractions before fishing was higher in the experimentally fished sites (T0), and was increased by trawling (T1). SumWing trawling increased the variability to a lesser degree (silt fraction: threefold, fine sand fraction: twofold), but its effect also occurred in deeper sediment layers (<4 cm). PulseWing trawling increased the variability in silt fraction (by a factors 3–5) and in fine sand fraction (by a factors 2–3) but its effect remained limited to the top layers (≤ 2 cm).

Modelled penetration depth

The seabed deformation following the passage of the nose of a wing-shaped foil is depicted in Figure 11. A number of simulations with different gear weights was conducted to construct a relationship with the average of penetration depths. The penetration depth of the nose varies according to weight following a nearly linear relationship between 1 000 and 2 000 kg submerged weight (Figure 12). The penetration depths vary between 2.2 and 2.5 cm for the SumWing trawl and between 1.7 and 1.95 cm for the PulseWing trawl. Numerical models were also run for a single electrode and a single tickler chain. Penetration depths varied between 1.5 and 1.9 cm with a mean of 1.7 cm for a single tickler chain while penetration depth of a

single electrode varied between 1.0 and 1.5 cm with a mean of 1.2 cm.

Modelled sediment mobilization

The amount of silt mobilized is estimated at 10.6 kg m^{-2} and 13.1 kg m^{-2} for SumWing trawl and PulseWing trawl, respectively. This corresponds to a mobilized sediment layer of 6.6 and 8.2 mm, respectively (assuming a porosity of 0.4). This difference is caused by the different silt fractions of the study sites. The hydrodynamic drag of both gears is very similar although the contribution of the different gear components differs (Table 3). Even though the SumWing trawl is towed at a higher speed (6 kn vs. 5), the

hydrodynamic drag of the lower netting panels is less than that of the PulseWing trawl. This is a result of the single twine used in the SumWing trawl and the higher number of panels fitted in the belly section of the PulseWing trawl (Supplementary Figure S3). The hydrodynamic drag of the SumWing gear (ground gear and tickler chains) is greater than that of the PulseWing trawl gear (ground gear and electrodes). The differences between the drag of the 2 types of noses of the wing-shaped foil may be directly attributed to their different towing speeds.

Total penetration depth

The total penetration depth of the gears is given by the sum of the erosion due to sediment mobilization (see “Modelled sediment mobilization” section, Table 3) and the mean depth of disturbance (see “Oxidized layer and depth of disturbance” section). Total penetration depth was estimated at 4.1 cm ($SD=0.9$ cm) and 1.8 cm ($SD=0.8$ cm) for the SumWing and the PulseWing trawl, respectively (Table 4). The variability (SD) in penetration depth is similar (see also penetration profiles in Figure 8), but occurs at different disturbance depths in the seabed.

Discussion

Our study has shown that the use of PulseWing trawls instead of SumWing trawls reduced most of the observed mechanical trawling impacts on the seabed for this substrate and area characteristics. The mobilization of sediment into the water column was comparable between both gears due to lighter trawl nets used in SumWing trawls, but penetration of the seabed by the PulseWing trawl was reduced by more than 50% in comparison to the SumWing trawl. Both trawling types caused tracks and homogenized the seabed topography without full recovery within 48 h, but seabed impacts of SumWing trawling were consistently higher than those of PulseWing trawling. The SumWing trawl penetrated into the deeper layers (subsurface layer; >2 cm) and thereby consistently flattened the surface boundary and consistently deepened the seabed along the trawled track. The seabed

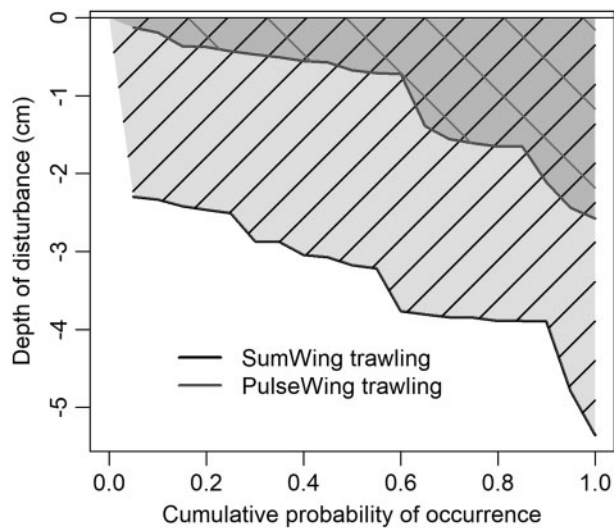


Figure 8. Depth of disturbance following SumWing trawling is deeper than following PulseWing trawling based on the assessment of the SPI images.

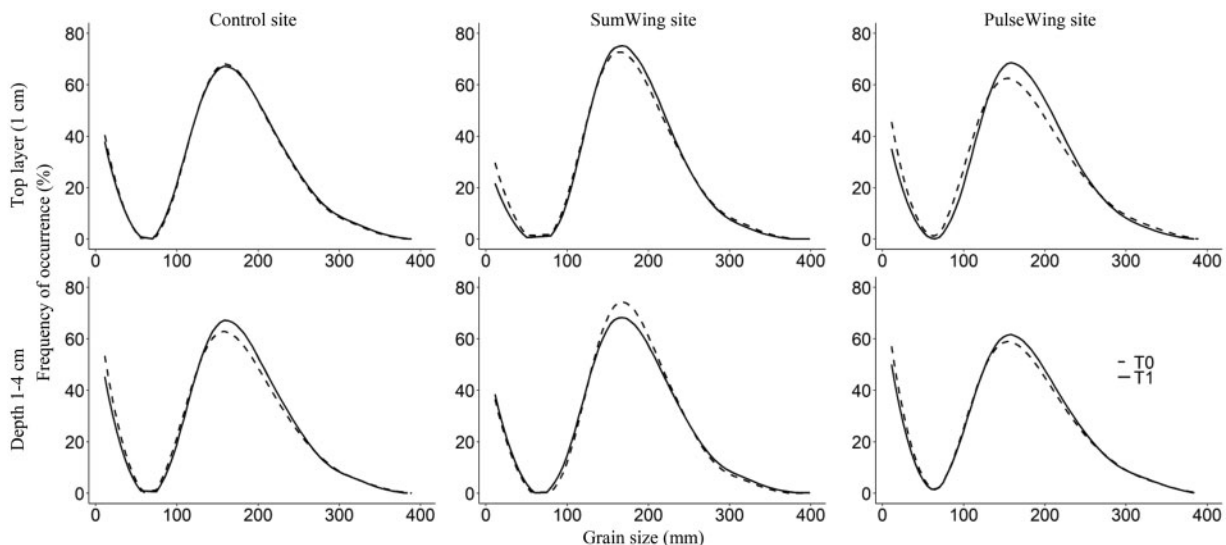


Figure 9. Particle size distributions at the top 1 cm of the seabed (upper row) and between 1 and 4 cm depth (lower row) before (T0, dashed line) and after (T1, solid line) experimental fishing in the control, SumWing trawl, and PulseWing trawl site. Depth categories were based on the mean depth of disturbance after SumWing and PulseWing trawling (Figure 8; Table 4).

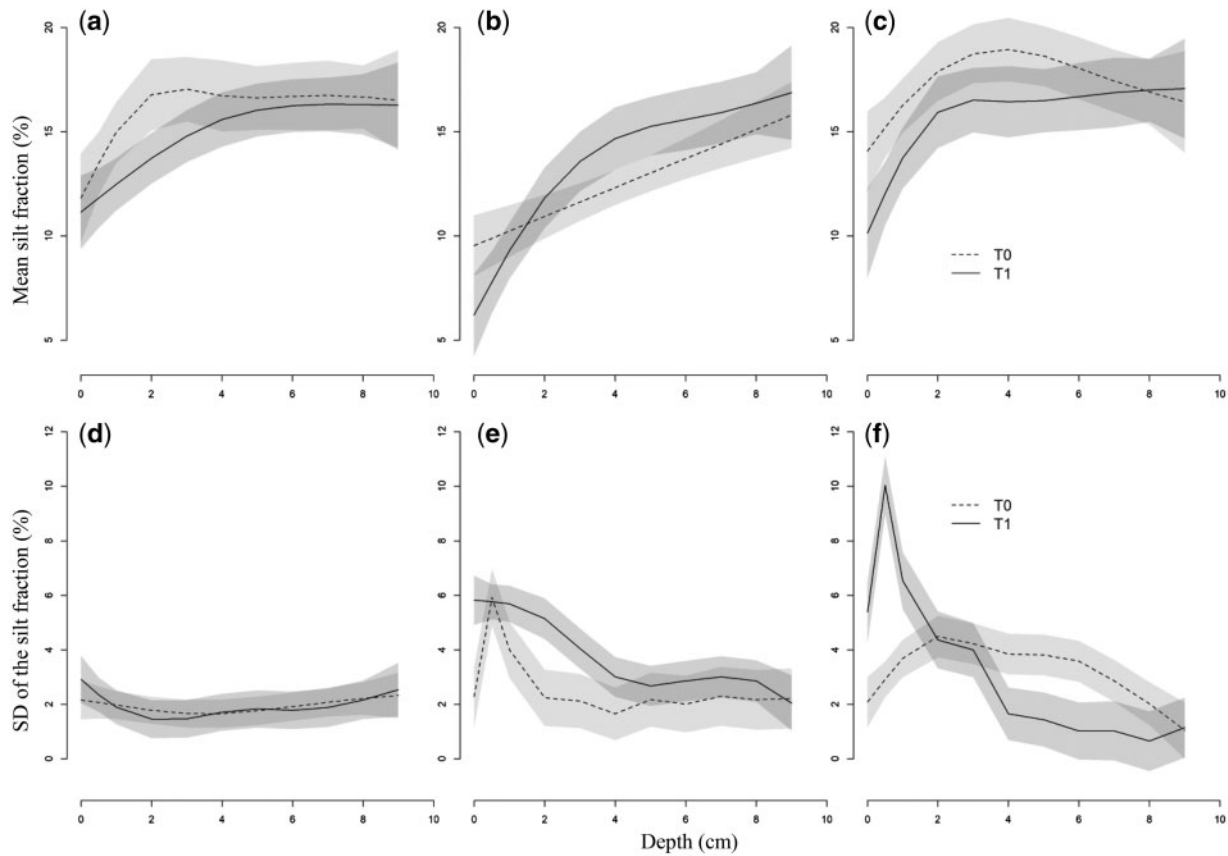


Figure 10. Predicted mean (upper panels) and SD (lower panels) of the silt fraction (expressed as a percentage) in function of depth of sampling in the seabed in (a) control, (b) SumWing, and (c) PulseWing trawl sites before and after fishing (T0, T1), based on Generalized Additive Models. Grey shaded areas delineate 95% confidence intervals.

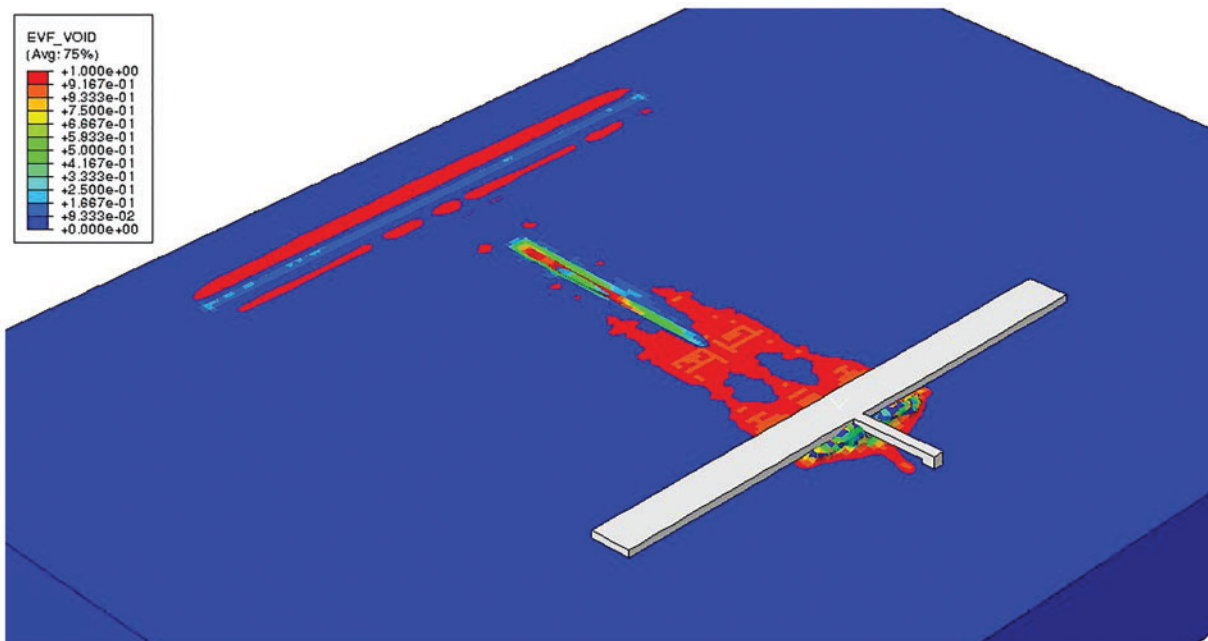


Figure 11. Deformation of the seabed through penetration of the nose of the wing-shaped foil used by the SumWing and the PulseWing trawl. Deformation was measured as the EVF, which tracks the flow of material through the Eulerian mesh. The value of EVF represents the portion of material filled; EVF = 1 indicates that the element is completely filled with the material and EVF = 0 indicates the element is devoid of the material. The wing-shaped foil can move through the Eulerian mesh without any resistance if its volume fraction is zero.

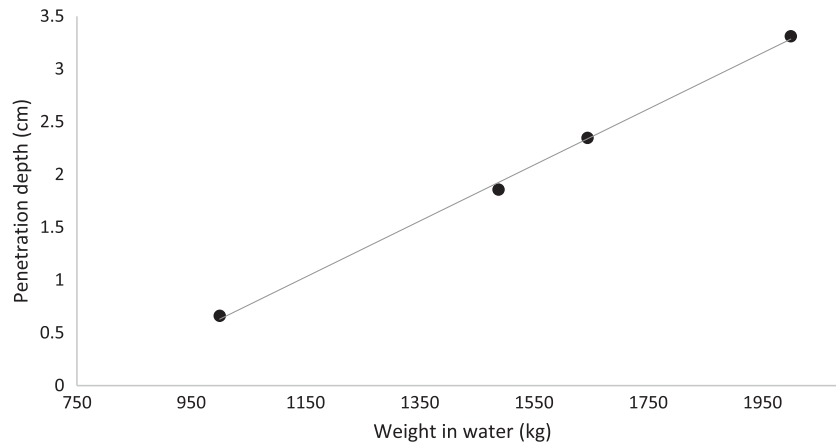


Figure 12. Modelled penetration depth (cm) of the nose of the wing-shaped foil as function of their respective weights in water. Penetration of the nose was 2.3 cm for the SumWing trawl, and 1.9 cm for the PulseWing trawl.

Table 3. Estimates of the hydrodynamic drag (N m^{-1}) and sediment mobilization (kg m^{-2}) from the netting panels, the ground gear assemblies, the noses of the wing-shaped foil, and the total gear assemblage of a SumWing and PulseWing trawls.

	Towing speed (kn)	Silt (%)	Netting	Ground gear assemblage	Noses	Total	
Hydrodynamic drag per metre swept (N m^{-1})							
SumWing trawl	6	–	1 995	1 986	84	3 817	
PulseWing trawl	5	–	3 021	722	59	3 802	
Mass of sediment mobilized per m^2 swept (kg m^{-2})							Sediment layer (mm)
SumWing trawl	6	9.3	5.1	5.1	0.4	10.6	6.6
PulseWing trawl	5	14.7	9.9	2.7	0.6	13.1	8.2

Table 4. Comparison of penetration depth of the nose of the wing-shaped foil, tickler chains and electrodes, and estimates of the deepening of seabed bathymetry, the depth of disturbance from SPI images, the depth of sediment reworking (particle size analysis) and the mobilized sediment layer following SumWing trawling and PulseWing trawling.

Parameter of seabed impact	Assessment technique	SumWing trawl	PulseWing trawl
Deepening of seabed bathymetry	MBES	1.5 (0.9)	0.9 (1.6)
Depth of disturbance	SPI	3.4 (0.9)	1.0 (0.8)
Depth of sediment reworking	Box corer samples	<4	<2
Penetration depth of the nose of the wing-shaped foil	Numerical model	2.3	1.9
Penetration depth of a single tickler chain or electrode	Numerical model	1.7	1.2
Mobilized sediment layer	Hydrodynamic model	0.7	0.8
Total penetration depth	Summation	4.1 (0.9)	1.8 (0.8)

The total penetration depth was based on the sum of the depth of disturbance and the mobilized sediment layer. All measurements are in cm. Estimates of MBES and SPI measurements and calculations of the total penetration depth are reported as the mean and their standard deviations between brackets. MBES, multi-beam echo sounder; SPI, Sediment Profile Imagery.

penetration by the PulseWing trawl varied between skimming off the top mm and penetrating into the subsurface layers, which resulted in a reduced impact on surface boundary roughness and a reduced and highly variable deepening of the seabed. Pulse trawling allowed recovery of the oxidized layer within 48 h, while this recovery was not observed within 48 h after SumWing trawling. The lower impact of the pulse trawl is mainly due to the use of electrodes instead of tickler chains. The observed reduction in penetration depth applies to the sediment characteristics of our study area; it may be less in coarser sediments and more in finer sediments. Our results corroborate an earlier study carried out in shallow fine sand habitat in the coastal zone of the southern North Sea (Depestele *et al.*, 2016), where the modelled

penetration depths and resultant trawl tracks by euro-cutter vessels were slightly shallower (see [Supplementary Table S1](#)). Further work comparing the mechanical, electrical, chemical, and biological effects of gears on varying substrates, habitats, and hydrographic conditions and associated effects on seabed status and functions will build a more integrated view of gear effects on the seabed overall (ICES, 2018).

Sediment mobilization

The sediment mobilization model predicts that the SumWing trawl mobilized about 1.6 mm less sediment into the water column than the pulse trawl. These results were supported by analysis of particle sizes in the top layers of the seabed, where a loss of

fine particles was lower following SumWing vs. PulseWing trawling (2.2% in the top 2 cm layer after passage of the SumWing as opposed to 2.8% following PulseWing trawling). The limited differences in sediment mobilization can be attributed to the higher median grain size and lower silt content in the SumWing site than in the PulseWing site and to the use of different netting material and twine thickness. The reduced sediment mobilization of the SumWing trawl net was compensated by the higher hydrodynamic drag and sediment mobilization resulting from the ground gear assemblage and the tickler chains. *Depestele et al. (2016)* found no differences in sediment mobilization between tickler-chain and PulseWing trawling. While sediment mobilization was comparable for trawls using tickler chains or pulse electrodes in both case studies, these results should not be directly extrapolated to the tickler-chain or pulse trawler fleet without prior knowledge of gear and operational characteristics of the fleet, such as twine thickness and towing speed.

Sediment mobilization also occurs naturally in the Frisian Front (*Amaro et al., 2007*). A drop in current velocities below a critical level along the slope of the Frisian Front causes deposition of silt and clay particles and creates a muddy area located to the northeast of the experimental sites (*Creutzberg et al., 1984*). The tidal ellipses in the Frisian Front area are mostly oriented along a W to E-NE line with a maximum velocity $<50 \text{ cm s}^{-1}$ (*van der Molen and de Swart, 2001*). Deposition of the finer particles from neighbouring sites could not be completely ruled out, but was expected to be limited, given the orientation of the tidal ellipses and the experimental sites along the depth contours. Natural movement of sand resulting from tidal or wave currents should not have influenced the deeper sediment layers at the time of the experiment. *Aldridge et al. (2015: 134)* calculated that the seabed in the Frisian Front is not frequently disturbed to a depth of 3 cm per year (1–20 times per year). Conversely, sediment in the top layer may have been active. Assuming a depth-mean tidal velocity of $<40 \text{ cm/s}$ during the experiment (*Davies and Furnes, 1980; Amaro et al., 2007*) and using median grain size to calculate seabed roughness resulted in a bed stress of $<0.14 \text{ Nm}^{-2}$ (*Soulsby, 1997*), which is below the critical bed stress for sediment movement (0.16 Nm^{-2}) (*Soulsby, 1997: 106–109*). These calculations use averaged values, which imply that critical bed stress may have been exceeded and may have influenced the top layers. However, the lack of differences in grain size distribution before and after trawling (T0 and T1) suggested that the observed impacts in the top 1 cm layer were due to trawling rather than natural sediment movements (*Figure 9*). We also expect that the larger sediment particles mobilized by the experimental trawling settled within the experimental sites (200 m wide and $\sim 250 \text{ m}$ apart, E–W orientation), given that mean volume concentration of mobilized sediment in the water column drops quickly, e.g. from $\sim 650 \mu\text{l/l}$ to $80 \mu\text{l/l}$ at distance of 25–65 m behind the trawl (*Fonteyne, 2000; Depestele et al., 2016*).

Seabed topography

The deepening of the trawl tracks altered seabed morphology. Large-scale topographical variation increases with increasing trawling intensities at scales larger than the width of the gear for beam trawls (*Depestele et al., 2016*). In this study, we show that micro-topographical variation within the trawled tracks decreased. BS analysis suggested a reduced seabed roughness (*Ferrini and Flood, 2006*) due to the flattening of sand ripples,

small pits, and mounds, which have also been noted following scallop dredging (*Currie and Parry, 1999; Gilkinson et al., 2003; O'Neill et al., 2013*) and otter trawling (*Eleftheriou and Robertson, 1992; Schwinghamer et al., 1998; Tuck et al., 1998; Mengual et al., 2016*).

SumWing trawling reduced the seabed roughness the most as tickler chains are towed in perpendicular direction to the towing direction and flatten the seabed across the trawl track (*Figure 5*). PulseWing trawling reduced BS less as the shallow indentations by the electrodes are caused in parallel direction to the towing direction (*Murray et al., 2016*). These observations resemble the small depressions caused by rock hopper gear used in otter trawls (*Humborstad et al., 2004*) or the furrows created by dredges (*Dolmer et al., 2001*). Visual assessment of underwater footage of electrodes of PulseWing trawls (ILVO, unpublished data) showed that the electrodes do not vibrate or quickly undulate but had a slow lateral motion, and as such flatten seabed features over $<25\%$ of the width of the affected trawl path. Underwater footage also suggested that the tension relief cords (*Supplementary Figures S1 and S2*) used in PulseWing trawling, are not in direct contact with the seabed. This hypothesis is confirmed by the variation of the bathymetrical changes in *Figure 4*, i.e. SumWing trawling smoothens the sediment topography more uniformly than PulseWing trawling. BS reduction in the control site was not substantial ($<1 \text{ dB}$) and may reflect the deposition of finer sediment particles on shell fragments or hard-bodied organisms, thereby reducing their potential to act as acoustic scatterers. Small slopes and bed-forms were present in the control site before and after fishing leading to a higher roughness and higher sound scattering (less absorption). These bed-form irregularities were lacking in the PulseWing and SumWing trawling sites following fishing (*Figure 5*), as was also confirmed by SPI analysis, i.e. the lower surface boundary roughness following trawling (*Figure 7*). BS analysis showed that the initial smoothing of the trawl tracks (T1) was rapidly counteracted by infaunal activity, i.e. within 24 h (T2–T4; *Figure 5; Table 1*) (*Briggs and Richardson, 1997*). Similarly, the SPI images showed that infaunal activity, along with re-establishment of chemical zonation, contributed to the re-establishment of the oxidized layers (*Figure 7*) (*Smith et al., 2003*). BS analysis shows that full re-establishment of the micro-topography was not achieved within 48 h following either SumWing or PulseWing trawling (*Figure 5*).

Depth of disturbance and sediment reworking

Sediment mobilization may lead to substantial sediment erosion and deepening of trawl tracks (*Dellapenna et al., 2006; Simpson and Watling, 2006*). *Depestele et al. (2016)* showed that SumWing trawling deepened the track more than would be expected from sediment mobilization alone. Indeed, our study confirms that the SumWing trawl deepened the track by 13.7 mm, which is more than the 6.6 mm of sediment that the model predicts would be put into the water column due to the hydrodynamic drag. Our study also showed that the deepening of the PulseWing trawl track (7.4 mm) was comparable to 8.2 mm of mobilized sediment predicted by the model. These results suggest that gear components, which are designed to interact with the sediment, such as tickler chains, which are designed to dig out flatfish from the sediment, cause a more profound effect on the seabed sediment than gear components, which are dragged over the seabed surface, such as pulse electrodes. In this study, we

examined these geotechnical interactions in more detail by looking at the depth to which particle size distribution and the oxidized layer were affected.

Particle size analysis showed that SumWing trawling affected the deeper layers, i.e. down to ~ 4 cm, whereas PulseWing trawl impacts were limited to the top layers. The depth profile of the silt and fine sand fractions after SumWing trawling (T1) intersected the depth profile before trawling (T0) (Figure 10b). The trend of the depth profile of silt and fine sand fractions after PulseWing trawling was, in contrast to SumWing trawling, not different from untrawled conditions for the deeper layers (1–4 cm). These trends suggest that SumWing trawling mixed fine sediment particles into the deeper layers while PulseWing trawling did not. This vertical mixing by SumWings reduced the vertical gradient in particle sizes, a trend typical of chronically disturbed fishing grounds (Mengual *et al.*, 2016). The deeper seabed impact of the SumWing trawl in particle size analysis was further supported by the SPI analysis, as the presence of mud clasts increased in the SPI images following SumWing trawling (Nilsson and Rosenberg, 2003) and the homogenized layer following SumWing trawling reached deeper than after PulseWing trawl passage.

The deeper depth of disturbance and sediment reworking resulted in deeper trawl tracks by the SumWing trawl than the PulseWing trawl. Increased sediment reworking may have also increased sediment compaction into the deeper layers. Sediment compaction implies that the dry bulk density increases after trawling, which may be measured directly (Pusceddu *et al.*, 2014) or suggested indirectly from estimates of seabed “hardness” in RoxAnn surveys (Fonteyne, 2000), from a decreased prism penetration of the SPI (Smith *et al.*, 2003) or from bathymetrical changes (this study). One plausible explanation of increased compaction is suggested by Durrieu de Madron *et al.* (2005). Pore water is released to the water column from deeper depths in the seabed than the resuspension of fine sediment particles which come only from the top few mm. Deeping of the trawl tracks may be further explained by the disruption of macrofaunal burrows and voids (Smith *et al.*, 2003), particularly when associated with high mortality rates of bioturbators (Gilkinson *et al.*, 2003). The short-term loss of burrows and voids created by bioturbators is also a likely hypothesis for the deepening of the trawl tracks and sediment compaction in our experiments, given the occurrences of infaunal bioturbators like *Echinocardium* spp. and *Callianassa* spp. in the SPI images and their importance in the Frisian Front (Amaro *et al.*, 2007; Duineveld *et al.*, 2007; Witbaard *et al.*, 2013). The deeper depth of disturbance by the SumWing trawl has likely caused higher mortality rates of infaunal organisms than the PulseWing trawl, since the mortality rate imposed by a bottom trawl is proportional to the penetration depth of the gear (Hiddink *et al.*, 2017; Sciberras *et al.*, 2018). Penetration depth was estimated by combining the measured depth of sediment disturbance and homogenization from SPI measurements with modelled depth of erosion due to sediment mobilization. The inferred reduction in mortality rate is related to the effect of mechanical disturbance, primarily due to the replacement of tickler chains. Whether electrical stimulation results in any additional mortality under marine circumstances is yet unknown, but laboratory evidence suggests that exposure to a pulse stimulus will not result in a measurable additional mortality (Soetaert *et al.*, 2015b, 2016; ICES, 2018).

Implications of the depth of disturbance

Trawling impacts in the top layers caused mobilization of fine sediment particles, which were advected with water currents. This process, known as winnowing, caused a progressive coarsening of surficial sediments and is mirrored in natural processes and stimulated by the activities of extreme bioturbators, which also release fine particles from the top layers and cause an upward coarsening trend (Singer and Anderson, 1984; Briggs and Richardson, 1997; Le Hir *et al.*, 2007; Olsgard *et al.*, 2008; Sciberras *et al.*, 2016). Various studies have demonstrated fine fraction winnowing of intensive long-term bottom trawling and dredging (Caddy, 1973; Trimmer *et al.*, 2005; Martín *et al.*, 2014; Mengual *et al.*, 2016; Payo-Payo *et al.*, 2017). Our short-term, acute impact study confirms these findings by demonstrating the causal link between the loss of fine sediment in the top layers of the fished sites in contrast to the control site (Figure 10). The winnowing effects may increase turbidity (Churchill *et al.*, 1988) and mobilize oxidized sediment particles and nutrients and in due course affect processes in the water column (Dounas *et al.*, 2007; Couceiro *et al.*, 2013).

Whereas both SumWing and PulseWing trawling reworked the top layers of the seabed, SumWing trawling also caused vertical mixing and homogenization of sediment particles in deeper layers. The replacement of the oxidized layer by a homogenized layer may further retard organic matter cycling by the shift from surficial aerobic to subsurface, anaerobic respiration (Trimmer *et al.*, 2005; Aldridge *et al.*, 2017). This homogenization does not occur in any natural processes and may have significant ecological implications to the stability of carbon mineralization and nutrient cycles (Mayer *et al.*, 1991; Duplisea *et al.*, 2001; Sciberras *et al.*, 2016). The deeper depth of disturbance following SumWing trawling also implied that recovery, such as the re-establishment of the oxidized layer, was slower than after disturbance caused by a PulseWing trawl. The inferred higher mortality of bioturbators could have contributed further to the slower recovery following SumWing trawling.

Supplementary data

Supplementary material is available at the ICESJMS online version of the manuscript.

Acknowledgements

We are grateful for the logistic support of VLIZ, the fishermen of TX43 and TX29 and crew members of RV ISIS and RV Simon Stevin during the sea trials and NIOZ for the use of their box corer. ADR and LRT were partly supported by the project “Impact assessment pulsvisserij”. We are indebted to the skippers and Eddy Buyvoets for drawing the net plans of the trawls. We thank John Aldridge for his insights in sediment transport in relation to natural dynamics; Bavo De Witte for conducting the particle size analysis; Daniel Benden for assisting SPI analyses; Miriam Levenson for English-language editing and Julie Bremner and Stefan Bolam for their critical review. We also wish to thank three anonymous reviewers for their constructive comments on earlier drafts of this manuscript.

Funding

This study was part-funded by the EU FP 7 project BENTHIS (grant no. 312088). It does not necessarily reflect the views of the

European Commission and does not anticipate the Commission's future policy in this area.

References

- Aldridge, J. N., Parker, E. R., Bricheno, L. M., Green, S. L., and van der Molen, J. 2015. Assessment of the physical disturbance of the northern European Continental shelf seabed by waves and currents. *Continental Shelf Research*, 108: 121–140.
- Aldridge, J. N., Lessin, G., Amoudry, L. O., Hicks, N., Klar, J. K., and Kitidis, V. 2017. Comparing benthic biogeochemistry at a sandy and a muddy site in the Celtic Sea using a model and observations. *Biogeochemistry*, 135: 155–182.
- Amaro, T., Duineveld, G., Bergman, M., Witbaard, R., and Scheffer, M. 2007. The consequences of changes in abundance of *Callianassa subterranea* and *Amphiura filiformis* on sediment erosion at the Frisian Front (south-eastern North Sea). *Hydrobiologia*, 589: 273–285.
- Bayse, S. M., Herrmann, B., Lenoir, H., Depestele, J., Polet, H., Vanderperren, E., and Verschuere, B. 2016. Could a T90 mesh codend improve selectivity in the Belgian beam trawl fishery? *Fisheries Research*, 174: 201–209.
- Beare, D., Rijnsdorp, A. D., Blaesberg, M., Damm, U., Egekvist, J., Fock, H., and Kloppmann, M. 2013. Evaluating the effect of fishery closures: lessons learnt from the Plaice Box. *Journal of Sea Research*, 84: 49–60.
- Bockelmann, F.-D., Puls, W., Kleeberg, U., Müller, D., and Emeis, K.-C. 2018. Mapping mud content and median grain-size of North Sea sediments—a geostatistical approach. *Marine Geology*, 397: 60–71.
- Briggs, K. B., and Richardson, M. D. 1997. Small-scale fluctuations in acoustic and physical properties in surficial carbonate sediments and their relationship to bioturbation. *Geo-Marine Letters*, 17: 306–315.
- Caddy, J. F. 1973. Underwater observations on tracks of dredges and trawls and some effects of dredging on a scallop ground. *Journal of the Fisheries Research Board of Canada*, 30: 173–180.
- Cashion, T., Al-Abdulrazzak, D., Belhabib, D., Derrick, B., Divovich, E., Moutopoulos, D. K., Noël, S.-L. *et al.* 2018. Reconstructing global marine fishing gear use: catches and landed values by gear type and sector. *Fisheries Research*, 206: 57–64.
- Churchill, J. H., Biscaye, P. E., and Aikman, F. 1988. The character and motion of suspended particulate matter over the shelf edge and upper slope off Cape Cod. *Continental Shelf Research*, 8: 789–809.
- Collie, J. S., Hall, S. J., Kaiser, M. J., and Poiner, I. R. 2000. A quantitative analysis of fishing impacts on shelf-sea benthos. *Journal of Animal Ecology*, 69: 785–798.
- Couceiro, F., Fones, G. R., Thompson, C. E. L., Statham, P. J., Sivyer, D. B., Parker, R., Kelly-Gerrey, B. A. *et al.* 2013. Impact of resuspension of cohesive sediments at the Oyster Grounds (North Sea) on nutrient exchange across the sediment–water interface. *Biogeochemistry*, 113: 37–52.
- Creutzberg, F., Wapenaar, P., Duineveld, G., and Lopez Lopez, N. 1984. Distribution and density of the benthic fauna in the southern North Sea in relation to bottom characteristics and hydrographic conditions. *Rapports et Procès-Verbaux des Réunions du Conseil Permanent International pour l'Exploration de la Mer*, 183: 101–110.
- Currie, D. R., and Parry, G. D. 1999. Impacts and efficiency of scallop dredging on different soft substrates. *Canadian Journal of Fisheries and Aquatic Sciences*, 56: 539–550.
- Dassault. 2014. Dassault Systems, 2014. SIMULA Abaqus Analysis User's Manual Version 6.14. <http://abaqus.software.polimi.it/v6.14/books/usb/default.htm> (last accessed 30 August 2018).
- Davies, A. M., and Furnes, G. K. 1980. Observed and computed M2 tidal currents in the North Sea. *Journal of Physical Oceanography*, 10: 237–257.
- de Haan, D., Fosseidengen, J. E., Fjellidal, P. G., Burggraaf, D., and Rijnsdorp, A. D. 2016. Pulse trawl fishing: characteristics of the electrical stimulation and the effect on behaviour and injuries of Atlantic cod (*Gadus morhua*). *ICES Journal of Marine Science*, 73: 1557–1569.
- de Jong, M. F., Baptist, M. J., Lindeboom, H. J., and Hoekstra, P. 2015. Relationships between macrozoobenthos and habitat characteristics in an intensively used area of the Dutch coastal zone. *ICES Journal of Marine Science*, 72: 2409–2422.
- Dellapenna, T. M., Allison, M. A., Gill, G. A., Lehman, R. D., and Warnken, K. W. 2006. The impact of shrimp trawling and associated sediment resuspension in mud dominated, shallow estuaries. *Estuarine, Coastal and Shelf Science*, 69: 519–530.
- Depestele, J., Courtens, W., Degraer, S., Haelters, J., Hostens, K., Leopold, M., Pinn, E. *et al.* 2014. Sensitivity assessment as a tool for spatial and temporal gear-based fisheries management. *Ocean & Coastal Management*, 102: 149–160.
- Depestele, J., Ivanović, A., Degrende, K., Esmaeili, M., Polet, H., Roche, M., Summerbell, K. *et al.* 2016. Measuring and assessing the physical impact of beam trawling. *ICES Journal of Marine Science*, 73: i15–i26.
- Dolmer, P., Kristensen, T., Christiansen, M. L., Petersen, M. F., Kristensen, P. S., and Hoffmann, E. 2001. Short-term impact of blue mussel dredging (*Mytilus edulis* L.) on a benthic community. *In Coastal Shellfish—A Sustainable Resource: Proceedings of the Third International Conference on Shellfish Restoration, Held in Cork, Ireland, 28 September–2 October 1999*, pp. 115–127. Ed. by G. Burnell. Springer Netherlands, Dordrecht.
- Dounas, C., Davies, I., Triantafyllou, G., Koulouri, P., Petihakis, G., Arvanitidis, C., Sourlatzis, G. *et al.* 2007. Large-scale impacts of bottom trawling on shelf primary productivity. *Continental Shelf Research*, 27: 2198–2210.
- Duineveld, G. C. A., Bergman, M. J. N., and Lavaleye, M. S. S. 2007. Effects of an area closed to fisheries on the composition of the benthic fauna in the southern North Sea. *ICES Journal of Marine Science*, 64: 899–908.
- Duplisea, D. E., Jennings, S., Malcolm, S. J., Parker, R., and Sivyer, D. B. 2001. Modelling potential impacts of bottom trawl fisheries on soft sediment biogeochemistry in the North Sea. *Geochemical Transactions*, 2: 112.
- Durrieu de Madron, X., Ferré, B., Le Corre, G., Grenz, C., Conan, P., Pujó-Pay, M., Buscail, R. *et al.* 2005. Trawling-induced resuspension and dispersal of muddy sediments and dissolved elements in the Gulf of Lion (NW Mediterranean). *Continental Shelf Research*, 25: 2387–2409.
- Eigaard, O. R., Bastardie, F., Breen, M., Dinesen, G. E., Hintzen, N. T., Laffargue, P., Mortensen, L. O. *et al.* 2016. Estimating seabed pressure from demersal trawls, seines, and dredges based on gear design and dimensions. *ICES Journal of Marine Science*, 73: i27–i43.
- Eigaard, O. R., Bastardie, F., Hintzen, N. T., Buhl-Mortensen, L., Buhl-Mortensen, P., Catarino, R., Dinesen, G. E. *et al.* 2017. The footprint of bottom trawling in European waters: distribution, intensity, and seabed integrity. *ICES Journal of Marine Science*, 74: 847–865.
- Eleftheriou, A., and Robertson, M. R. 1992. The effects of experimental scallop dredging on the fauna and physical environment of a shallow sandy community. *Netherlands Journal of Sea Research*, 30: 289–299.
- Esmaeili, M., and Ivanović, A. 2014. Numerical modelling of bottom trawling ground gear element on the seabed. *Ocean Engineering*, 91: 316–328.
- Esmaeili, M., and Ivanović, A. 2015. Analytical and numerical modelling of non-driven disc on friction material. *Computers and Geotechnics*, 68: 208–219.
- EU. 2017. Commission Decision (EU) 2017/848 of 17 May 2017 laying down criteria and methodological standards on good environmental status of marine waters and specifications and

- standardised methods for monitoring and assessment, and repealing Decision 2010/477/EU. *Official Journal of the European Union*. L125/43. 32 pp. <http://eur-lex.europa.eu/legal-content/EN/TXT/PDF/?uri=CELEX:32017D0848&from=EN>.
- FAO. (2016) The State of World Fisheries and Aquaculture 2018. FAO, Rome.
- Ferrini, V. L., and Flood, R. D. 2006. The effects of fine-scale surface roughness and grain size on 300 kHz multibeam backscatter intensity in sandy marine sedimentary environments. *Marine Geology*, 228: 153–172.
- Fonteyne, R. 2000. Physical impact of beam trawls on seabed sediments. *In* The Effects of Fishing on Non-Target Species and Habitats: Biological, Conservation and Socio-Economic Issues, pp. 15–36. Ed. by M. J. Kaiser and S. J. de Groot. Fishing News Books. Blackwell Science, Oxford.
- Germano, J. D., Rhoads, D. C., Valente, R. M., Carey, D. A., and Solan, M. 2011. The use of sediment profile imaging (SPI) for environmental impact assessments and monitoring studies: lessons learned from the past four decades. *In* Oceanography and Marine Biology: An Annual Review, 49, pp. 235–297. Ed. by R. N. Gibson, R. J. A. Atkinson, and J. D. M. Gordon. CRC Press Taylor & Francis Group, Boca Raton, FL.
- Gilkinson, K., Paulin, M., Hurley, S., and Schwinghamer, P. 1998. Impacts of trawl door scouring on infaunal bivalves: results of a physical trawl door model/dense sand interaction. *Journal of Experimental Marine Biology and Ecology*, 224: 291–312.
- Gilkinson, K. D., Fader, G. B. J., Gordon, J., Charron, R., McKeown, D., Roddick, D., Kenchington, E. L. R. *et al.* 2003. Immediate and longer-term impacts of hydraulic clam dredging on an offshore sandy seabed: effects on physical habitat and processes of recovery. *Continental Shelf Research*, 23: 1315–1336.
- Haasnoot, T., Kraan, M., and Bush, S. R. 2016. Fishing gear transitions: lessons from the Dutch flatfish pulse trawl. *ICES Journal of Marine Science*, 73: 1235–1243.
- HfK Engineering. 2018. HfK Engineering Website [online]. www.sumwing.nl (last accessed 3 July 18).
- Hiddink, J., Jennings, S., Sciberras, M., Szostek, C., Hughes, K., Ellis, N., Rijnsdorp, A. D. *et al.* 2017. Global analysis of depletion and recovery of seabed biota following bottom trawling disturbance. *Proceedings of the National Academy of Sciences*, 114: 8301–8306.
- Hoaglin, D. C., and Iglewicz, B. 1987. Fine-tuning some resistant rules for outlier labeling. *Journal of the American Statistical Association*, 82: 1147–1149.
- Hoerner, S. F. 1965. *Fluid-Dynamic Drag*. Hoerner, New Jersey.
- Humborstad, O.-B., Nøttestad, L., Løkkeborg, S., and Rapp, H. T. 2004. RoxAnn bottom classification system, sidescan sonar and video-sledge: spatial resolution and their use in assessing trawling impacts. *ICES Journal of Marine Science*, 61: 53–63.
- ICES. 2018. Report of the Working Group on Electric Trawling (WGELECTRA). ICES Report WGELECTRA 2018 17–19 April 2018. IJmuiden, The Netherlands. 155 pp.
- Ifremer. 2016. <http://flotte.ifremer.fr/Presentation-de-la-flotte/Logiciels-embarques/SonarScope> (last accessed 23 February 2018).
- Ivanović, A., and O'Neill, F. G. 2015. Towing cylindrical fishing gear components on cohesive soils. *Computers and Geotechnics*, 65: 212–219.
- Kaiser, M. J., Clarke, K. R., Hinz, H., Austen, M. C. V., Somerfield, P. J., and Karakassis, I. 2006. Global analysis of response and recovery of benthic biota to fishing. *Marine Ecology-Progress Series*, 311: 1–14.
- Kaiser, M. J., Hilborn, R., Jennings, S., Amaroso, R., Andersen, M., Balliet, K., Barratt, E. *et al.* 2016. Prioritization of knowledge-needs to achieve best practices for bottom trawling in relation to seabed habitats. *Fish and Fisheries*, 17: 637–663.
- Knights, A. M., Piet, G. J., Jongbloed, R. H., Tamis, J. E., White, L., Akoglu, E., Boicenco, L. *et al.* 2015. An exposure-effect approach for evaluating ecosystemwide risks from human activities. *ICES Journal of Marine Science*, 72: 1105–1115.
- Kroodsmas, D. A., Mayorga, J., Hochberg, T., Miller, N. A., Boerder, K., Ferretti, F., Wilson, A. *et al.* 2018. Tracking the global footprint of fisheries. *Science*, 359: 904–908.
- Le Hir, P., Monbet, Y., and Orvain, F. 2007. Sediment erodability in sediment transport modelling: can we account for biota effects? *Continental Shelf Research*, 27: 1116–1142.
- Lindeboom, H. J., and de Groot, S. J. 1998. The effects of different types of fisheries on the North Sea and Irish Sea benthic ecosystems. NIOZ-Rapport 1998-1/RIVO/DLO Report C003/98. 404 pp.
- Løkkeborg, S. 2007. Insufficient understanding of benthic impacts of trawling is due to methodological deficiencies. A reply to Gray *et al.* (2006). *Marine Pollution Bulletin*, 54: 494–496.
- MacLennan, D. N. 1981. The drag of four-panel demersal trawls. *Fisheries Research*, 1: 23–33.
- Martín, J., Puig, P., Palanques, A., and Giamportone, A. 2014. Commercial bottom trawling as a driver of sediment dynamics and deep seascapes evolution in the Anthropocene. *Anthropocene*, 7: 1–15.
- Mayer, L. M., Schick, D. F., Findlay, R. H., and Rice, D. L. 1991. Effects of commercial dragging on sedimentary organic matter. *Marine Environmental Research*, 31: 249–261.
- Mengual, B., Cayocca, F., Le Hir, P., Draye, R., Laffargue, P., Vincent, B., and Garlan, T. 2016. Influence of bottom trawling on sediment resuspension in the 'Grande-Vasière' area (Bay of Biscay, France). *Ocean Dynamics*, 66: 1181–1207.
- Mills, C. M., Townsend, S. E., Jennings, S., Eastwood, P. D., and Houghton, C. A. 2007. Estimating high resolution trawl fishing effort from satellite-based vessel monitoring system data. *ICES Journal of Marine Science*, 64: 248–255.
- Murray, F., Copland, P., Boulcott, P., Robertson, M., and Bailey, N. 2016. Impacts of electrofishing for razor clams (*Ensis* spp.) on benthic fauna. *Fisheries Research*, 174: 40–46.
- Nilsson, H. C., and Rosenberg, R. 2003. Effects on marine sedimentary habitats of experimental trawling analysed by sediment profile imagery. *Journal of Experimental Marine Biology and Ecology*, 285–286: 453–463.
- Oberle, F. K. J., Storlazzi, C. D., and Hanebuth, T. J. J. 2016. What a drag: quantifying the global impact of chronic bottom trawling on continental shelf sediment. *Journal of Marine Systems*, 159: 109–119.
- Oberle, F. K. J., Puig, P., and Martín, J. 2018. Fishing activities. *In* Submarine Geomorphology, pp. 503–534. Ed. by A. Micallef, S. Krastel, and A. Savini. Springer International Publishing, Cham, Switzerland.
- Olsgard, F., Schaanning, M. T., Widdicombe, S., Kendall, M. A., and Austen, M. C. 2008. Effects of bottom trawling on ecosystem functioning. *Journal of Experimental Marine Biology and Ecology*, 366: 123–133.
- O'Neill, F. G., Robertson, M., Summerbell, K., Breen, M., and Robinson, L. A. 2013. The mobilisation of sediment and benthic infauna by scallop dredges. *Marine Environmental Research*, 90: 104–112.
- O'Neill, F. G., and Ivanović, A. 2016. The physical impact of towed demersal fishing gears on soft sediments. *ICES Journal of Marine Science*, 73: i5–i14.
- O'Neill, F. G., and Summerbell, K. D. 2016. The hydrodynamic drag and the mobilisation of sediment into the water column of towed fishing gear components. *Journal of Marine Systems*, 164: 76–84.
- Palanques, A., Guillen, J., and Puig, P. 2001. Impact of bottom trawling on water turbidity and muddy sediment of an unfished continental shelf. *Limnology and Oceanography*, 46: 1100–1110.

- Payo-Payo, M., Jacinto, R. S., Lastras, G., Rabineau, M., Puig, P., Martin, J., Canals, M. *et al.* 2017. Numerical modeling of bottom trawling-induced sediment transport and accumulation in La Fonera submarine canyon, northwestern Mediterranean Sea. *Marine Geology*, 386: 107–125.
- Pilskaln, C. H., Churchill, J. H., and Mayer, L. M. 1998. Resuspension of sediment by bottom trawling in the Gulf of Maine and potential geochemical consequences. *Conservation Biology*, 12: 1223–1229.
- Pitcher, C. R., Ellis, N., Jennings, S., Hiddink, J. G., Mazor, T., Kaiser, M. J., Kangas, M. I. *et al.* 2017. Estimating the sustainability of towed fishing-gear impacts on seabed habitats: a simple quantitative risk assessment method applicable to data-limited fisheries. *Methods in Ecology and Evolution*, 8: 472–480.
- Puig, P., Canals, M., Company, J., Martin, J., Amblas, D., Lastras, G., and Palanques, A. 2012. Ploughing the deep sea floor. *Nature*, 489: 286–289.
- Pusccheddu, A., Bianchelli, S., Martin, J., Puig, P., Palanques, A., Masque, P., and Danovaro, R. 2014. Chronic and intensive bottom trawling impairs deep-sea biodiversity and ecosystem functioning. *Proceedings of the National Academy of Sciences of the United States of America*, 111: 8861–8866.
- Rhoads, D. C., and Cande, S. 1971. Sediment profile camera for *in situ* study of organisms-sediment relations. *Limnology and Oceanography*, 16: 110–114.
- Rijnsdorp, A. D., Poos, J. J., Quirijns, F., HilleRisLambers, R., de Wilde, J. W., and den Heijer, W. M. 2008. The arms race between fishers. *Journal of Sea Research*, 60: 126–138.
- Rijnsdorp, A. D., Bastardie, F., Bolam, S. G., Buhl-Mortensen, L., Eigaard, O. R., Hamon, K. G., Hiddink, J. G. *et al.* 2016. Towards a framework for the quantitative assessment of trawling impacts on the seabed and benthic ecosystem. *ICES Journal of Marine Science*, 73: i127–i138.
- Schwinghamer, P., Gordon, D. C., Rowell, T. W., Prena, J., McKeown, D. L., Sonnichsen, G., and Guigné, J. Y. 1998. Effects of experimental otter trawling on surficial sediment properties of a sandy-bottom ecosystem on the Grand Banks of Newfoundland. *Conservation Biology*, 12: 1215–1222.
- Sciberras, M., Parker, R., Powell, C., Robertson, C., Kröger, S., Bolam, S., and Hiddink, J. 2016. Impacts of bottom fishing on the sediment infaunal community and biogeochemistry of cohesive and non-cohesive sediments. *Limnology and Oceanography*, 61: 2076–2089.
- Sciberras, M., Hiddink, J. G., Jennings, S., Szostek, C., Hughes, K. M., Kneafsey, B., Clarke, L. J. *et al.* 2018. Response of benthic fauna to experimental bottom fishing: a global meta-analysis. *Fish and Fisheries*. <https://doi.org/10.1111/faf.12283>.
- Simpson, A. W., and Watling, L. 2006. An investigation of the cumulative impacts of shrimp trawling on mud-bottom fishing grounds in the Gulf of Maine: effects on habitat and macrofaunal community structure. *ICES Journal of Marine Science*, 63: 1616–1630.
- Singer, J. K., and Anderson, J. B. 1984. Use of total grain-size distributions to define bed erosion and transport for poorly sorted sediment undergoing simulated bioturbation. *Marine Geology*, 57: 335–359.
- Smith, C. J., Rumohr, H., Karakassis, I., and Papadopoulou, K. N. 2003. Analysing the impact of bottom trawls on sedimentary seabeds with sediment profile imagery. *Journal of Experimental Marine Biology and Ecology*, 285–286: 479–496.
- Soetaert, M., Decostere, A., Polet, H., Verschueren, B., and Chiers, K. 2015a. Electrotrawling: a promising alternative fishing technique warranting further exploration. *Fish and Fisheries*, 16: 104–124.
- Soetaert, M., Chiers, K., Duchateau, L., Polet, H., Verschueren, B., and Decostere, A. 2015b. Determining the safety range of electrical pulses for two benthic invertebrates: brown shrimp (*Crangon* L.) and ragworm (*Alitta virens* S.). *ICES Journal of Marine Science*, 72: 973–980.
- Soetaert, M., Verschueren, B., Chiers, K., Duchateau, L., Polet, H., and Decostere, A. 2016. Laboratory study of the impact of repetitive electrical and mechanical stimulation on brown shrimp *Crangon crangon*. *Marine and Coastal Fisheries*, 8: 404–411.
- Solan, M., and Kennedy, R. 2002. Observation and quantification of *in situ* animal-sediment relations using time-lapse sediment profile imagery (t-SPI). *Marine Ecology Progress Series*, 228: 179–191.
- Solan, M., Wigham, B. D., Hudson, I. R., Kennedy, R., Coulon, C. H., Norling, K., Nilsson, H. C. *et al.* 2004. *In situ* quantification of bioturbation using time-lapse fluorescent sediment profile imaging (f-SPI), luminophore tracers and model simulation. *Marine Ecology Progress Series*, 271: 1–12.
- Soulsby, R. L. 1997. *Dynamics of Marine Sands*. Thomas Telford Publications, London. 249 pp.
- Stanev, E. V., Dobrynin, M., Pleskachevsky, A., Grayek, S., and Günther, H. 2009. Bed shear stress in the southern North Sea as an important driver for suspended sediment dynamics. *Ocean Dynamics*, 59: 183–194.
- Statham, P. J., Homoky, W. B., Parker, E. R., Klar, J. K., Silburn, B., Poulton, S. W., Kröger, S. *et al.* 2018. Extending the applications of sediment profile imaging to geochemical interpretations using colour. *Continental Shelf Research*, in press. <https://doi.org/10.1016/j.csr.2017.12.001>.
- Teal, L. R., Bulling, M. T., Parker, E. R., and Solan, M. 2008. Global patterns of bioturbation intensity and mixed depth of marine soft sediments. *Aquatic Biology*, 2: 207–218.
- Teal, L. R., Parker, R., Fones, G., and Solan, M. 2009. Simultaneous determination of *in situ* vertical transitions of color, pore-water metals, and visualization of infaunal activity in marine sediments. *Limnology and Oceanography*, 54: 1801–1810.
- Trimmer, M., Petersen, J., Sivyer, D. B., Mills, C., Young, E., and Parker, E. R. 2005. Impact of long-term benthic trawl disturbance on sediment sorting and biogeochemistry in the southern North Sea. *Marine Ecology Progress Series*, 298: 79–94.
- Tuck, I. D., Hall, S. J., Robertson, M. R., Armstrong, E., and Basford, D. J. 1998. Effects of physical trawling disturbance in a previously unfished sheltered Scottish sea loch. *Marine Ecology Progress Series*, 162: 227–242.
- Tyler-Walters, H., Rogers, S. I., Marshall, C. E., and Hiscock, K. 2009. A method to assess the sensitivity of sedimentary communities to fishing activities. *Aquatic Conservation: Marine and Freshwater Ecosystems*, 19: 285–300.
- Uhlmann, S. S., Theunynck, R., Ampe, B., Desender, M., Soetaert, M., and Depestele, J. 2016. Injury, reflex impairment, and survival of beam-trawled flatfish. *ICES Journal of Marine Science*, 73: 1244–1254.
- van der Molen, J., and de Swart, H. E. 2001. Holocene tidal conditions and tide-induced sand transport in the southern North Sea. *Journal of Geophysical Research: Oceans*, 106: 9339–9362.
- van Marlen, B., Wiegierinck, J. A. M., van Os-Koomen, E., and van Barneveld, E. 2014. Catch comparison of pulse trawls and a tickler chain beam trawl. *Fisheries Research*, 151: 57–69.
- Wickham, H. 2009. *ggplot2: Elegant Graphics for Data Analysis*. Springer-Verlag, New York.
- Witbaard, R., Lavaleye, M. S. S., Duineveld, G. C. A., and Bergman, M. J. N. 2013. Atlas of the megabenthos (incl. small fish) on the Dutch Continental Shelf of the North Sea. NIOZ-Report 2013-4. 243 pp.
- Wood, S. 2011. Package “mgcv”. R Package Library, Version 1.8-15. <http://cran.r-project.org> (last accessed 23 February 2018).
- Xu, Z., and Huang, S. 2014. Numerical investigation of mooring line damping and the drag coefficients of studless chain links. *Journal of Marine Science and Application*, 13: 76–84.